

UC San Diego

UC San Diego Electronic Theses and Dissertations

Title

Boundary element methods for viscous flow with applications in microcantilever array

Permalink

<https://escholarship.org/uc/item/8js6r3rg>

Author

He, Putian

Publication Date

2019

Peer reviewed|Thesis/dissertation

UNIVERSITY OF CALIFORNIA SAN DIEGO

Boundary element methods for viscous flow with applications in microcantilever array

A Thesis submitted in partial satisfaction of the requirements
for the degree Master of Science

in

Bioengineering

by

Putian He

Committee in charge:

Professor Ratneshwar Lal, Chair
Professor Gert Cauwenberghs
Professor Peter Franks

2019

Copyright
Putian He, 2019
All rights reserved.

The Thesis of Putian He is approved, and it is acceptable in quality and form for publication on microfilm and electronically:

Chair

University of California San Diego

2019

DEDICATION

To my parents for their unconditional love and support.

EPIGRAPH

*“To see a World in a Grain of Sand
And a Heaven in a Wild Flower,
Hold Infinity in the palm of your hand
And Eternity in an hour.”*

—William Blake

TABLE OF CONTENTS

Signature Page	iii
Dedication	iv
Epigraph	v
Table of Contents	vi
List of Figures	viii
Acknowledgments	ix
Vita	x
Abstract of the Thesis	xi
Chapter 1 Introduction	1
1.1 Background	2
1.2 Outline	4
Chapter 2 Equations of motion	6
2.1 Overview of equations of motion	6
2.2 Nondimensionalization	9
2.3 Spatial discretization	10
2.4 Temporal discretization	11
2.5 Algorithms overview	12
Chapter 3 Microhydrodynamics	13
3.1 Principles of mass and momentum conservation	13
3.2 Fundamental solutions of Stokes equations	15
3.3 Boundary integral equation	18
3.4 Singularity regularization	20
Chapter 4 Boundary Element method	21
4.1 Nystrom method	22
4.2 Weighted residual methods	23
4.3 Geometric interpolations	25
4.4 Numerical integration	26
4.5 Matrix form	29
4.6 N-body interaction	30
4.7 Summary of the mobility matrix	31
Chapter 5 Results and Discussions	33
5.1 Passive cantilevers under a Couette flow	33
5.2 Actively-driven cantilevers array in stagnant fluids	37
5.3 The effect of the wall	40

Chapter 6 Conclusions	43
Appendixes	44
A. Equation of motion without beam inertia	44
B. Fundamental solutions of Stokes equations in free space	46
C. Source dipole, force dipole, and multipole	49
D. Boundary integral equations	51
E. Geometric interpolations	54
F. Mathematical lemmas	56
References.....	57

LIST OF FIGURES

Figure 1	Schematic diagram of an elastic beam	7
Figure 2	B-spline basis function	27
Figure 3	A 3-by-3 microcantilever array undergoes a shear flow with Young's modulus, $E = 160$ GPa	34
Figure 4	A 3-by-3 microcantilever array immersed in fluids with different viscosity ranging from 0.3 to 3 cP for physiological fluids	35
Figure 5	A 3-by-3 microcantilever array undergoes a shear flow with young's modulus, $E = 1.60$ GPa	36
Figure 6	Spatial convergence and order of accuracy test for figure 3	37
Figure 7	A 3-by-3 microcantilever array actively driven in stagnant fluids with young's modulus, $E = 160$ GPa	39
Figure 8	Spatial convergence and order of accuracy test for figure 7 with a driving force period 21 secs	40
Figure 9	Spatial convergence and order of accuracy test for figure 7 with a driving force period 1 min	40
Figure 10	A 10-by-10 actively-driven microcantilevers array with/ without the effect of the wall in stagnant fluids	41
Figure 11	Snapshots of a complete driving cycle of figure 10 with the effect of the wall	42

ACKNOWLEDGMENTS

I owe my deepest gratitude to my advisor Professor Ratneshwar Lal. I'm extremely grateful to him for taking me under his lab, generously providing me with office spaces, and the valuable time he has spent in advising me. His continuous engagement has encouraged me to learn and helped me grow as a researcher. I am grateful for Professor Gerts Cawenberghs because of his great course on "mathematical methods" where I was introduced to the concept of Green's function and finite element methods. I am grateful for Professor Peter Franks because of his great 'Biological-physical interactions' course introduced me to the field of low Reynold number processes and biological oceanography.

VITA

2019-2017 Master of Science, Jacobs School of Engineering,
University of California San Diego, USA

2017-2014 Bachelor of Engineering (1st class honours), Royal School
of Mines, Imperial College London, UK

Associateship of the City and Guilds of London Institute

FIELDS OF STUDY

Major Fields: Biomedical Engineering
Fluid Mechanics
Dynamical System

ABSTRACT OF THE THESIS

Boundary element methods for viscous flow with applications in microcantilever array

by

Putian He

Master of Science in Bioengineering

University of California San Diego, 2019

Professor Ratneshwar Lal, Chair

Fluid-structure interactions at microscale are ubiquitous in biology and engineering. Understanding the complex micromechanical phenomena arises from the interplay between inertia, elastic, and viscous forces on the microstructures are computationally formidable tasks but essential. At zero Reynold number asymptotic limit, fluids are dominated by viscosity, and the drag force changes linearly with local fluid speed, which exists analytical Green's functions for the governing Stokes equations. In this thesis, the N-body hydrodynamic interactions of Euler-Bernoulli elastic beams immersed in viscous, incompressible fluids at zero Reynold number limit are solved computationally. A numerical recipe and program based on the symmetric Galerkin boundary element method are developed in Matlab for solving the boundary integral equations. In

the end, up to one hundred hydrodynamically fully coupled elastic beams were able to be solved efficiently on a standard desktop personal computer. These microstructures simulation could serve as the numerical basis for understanding how the macroscopic transport and rheological property is modified at the vicinity of cantilever arrays, and also as viscosity and flow sensors for various engineering applications.

Chapter 1 Introduction

Many interesting bioengineering problems involved a large number of slender elastic structures immersed in fluids at small scales. One example of such a system is liquid-state biopolymers in the cytoplasm, such as DNA, proteins, actin filament, and microtubules. Their hydrodynamic effect has been widely investigated, and a great deal of effort has been devoted to the study of protein-polymer aggregation under different flow field environments [1]. The long-range hydrodynamic interaction is especially dominant in a highly crowded cellular environment. For example, beta-amyloid peptide aggregation in physiological environments is strongly linked to the pathogenesis of Alzheimer's disease [2]. It is crucial to understand its formation mechanism under the physiological condition to develop effective drug inhibition mechanisms. Also, unlike the traditionally passive polymers reacting to the external flow field with disturbances, the biologically-active polymers have internal stress-generating mechanisms as a result of actively converting biochemical energy into mechanical work and electrical potential, therefore generating novel macroscale collective and emergent behavior. In the ocean, examples of such emergent macroscale systems due to active microstructures could also be found in the vertical migrations of zooplankton. The wakes of the individual zooplanktons coalesce to form a large-scale downward jet during their upward vertical migration. Recent studies [3] show that the collective vertical migration of zooplanktons can generate aggregation-scale eddies comparable to the length scales of stratification in the ocean, resulting in biologically-generated turbulent mixing contributing to nutrient transport. The immersed slender bodies could also be found in engineering applications such as the microcantilever probes immersed in the microfluidic devices, which has been demonstrated as novel velocimetry to measure submicron scales velocity profiles using silicon 'whiskers' [4] [5]. Also, similar microcantilevers-based systems

have been used as viscosity sensors [6] and mass resonators by exploring the microscale fluid-structure interaction phenomena. Results from these studies [4–6] are essential for understanding the control and characterization of microscale and nanoscale liquid flows in microfluidic devices such as multiphase transport and mixing effect in the microfluidic system.

1.1. Background

In the above systems, the dynamics of the immersed microstructures had played a significant role in the complex interactions leading to emergent phenomena. Fluids would exert forces on the solid structure, and the structural deformation would alter the path of the flow. The two-way coupling is a result of balancing hydrodynamic traction at the boundary surface by satisfying the no-slip boundary condition. One method that has been employed to study the fluid-structure interaction problems is known as the immersed boundary method [7], which was initially developed by Peskin to study the flow pattern around the biological heart valves. The method was created using two separated overlaying computational grids which one for fluids and one for structures. The interactions are achieved through forces and velocity interpolation between two computational grids, which eliminated the need for generating high-cost time-evolving body conforming-mesh such as standard methods used in COMSOL and ANSYS commercial software. Nevertheless, the computation for incompressible fluid is still costly in three dimensions, since the pressure term is a Lagrange multiplier in incompressible NS equations formulation and can only be solved iteratively by satisfying the continuity equation constraints, and the large degree of freedom in the numerical equations due to 3D volumetric discretization.

Microscale flow phenomena dominated by viscosity, in many cases, could be modeled by the Stokes equations at zero Reynold number limit, which has known fundamental solutions satisfying the continuity equation by their construction. The solutions can then be reformulated as a boundary integral equation by solving the given boundary conditions at the boundary of the domain only rather than computing the equation throughout the volumetric space, which reduced the degrees of freedom in the numerical equations. Once the unknown boundary variables are solved, the integral equation can be used to evaluate the solutions directly at any point in the volumetric domain as a post-processing step. There are two general approaches to discretize and solve for the boundary integral equation. In the Nystrom method, one can discretize the whole integral directly using quadrature points, and the variables discretization are collocated at the same points. However, in this approach, the discretization of variables and integral are implicitly coupled. For example, if one wants to reduce the variables discretization in the integral equation, the quadrature discretization for integrals also has to be reduced. And if more quadrature points are desired for integrals, the variables discretization also will have to be increased, which will introduce unnecessary degrees of freedom in the discretized integral equation.

Boundary element method (BEM) could alleviate this issue by decoupling the variables discretization and numerical quadrature [8]. BEM works by decomposing the variables of interests into locally supported continuous basis functions, and thereby compute the integrals of basis function and fundamental solutions over locally-supported elements only. The integrated Green's function elements connect pairs of source and field element defined by a global matrix. Also, it will be more effective and accurate to break down the domain into smaller subdomains and perform local integration on each subdomain using higher-order quadrature.

1.2. Outline

In this thesis, we study the microscale fluid-structure interaction of multiple slender elastic bodies immersed in three-dimensional stokes flow bounded by a rigid wall. The beams are considered to be elastic and inextensible with constitutive relations modeled by the Euler-Bernoulli equation [9]. The naturally straight cantilevers are modeled in such a way that any deviation from the equilibrium position will produce internal elastic forces to drive them back to natural shapes. Also, the aspect ratio of length to the radius of these slender structures ranges from ten to thousands. It is computationally more advantageous to consider only the centerline of the slender structures so that the boundary integral equation can be formulated as a line integral of fundamental solutions in three dimensions. Although the collocation method is the standard method used in the boundary element method to discretize the integral equation, we implemented a linear symmetric Galerkin method [10] to discretize the integral equation and solve for the hydrodynamic boundary forces to satisfy no-slip boundary conditions on the beams. Since the numerical equations in matrix form generated by the Galerkin method are symmetric, in the setup with multiple beams interaction, we only need to compute the upper triangular part of the global square matrix and flip it over the diagonal to retain the full matrix in the end. We also implemented a mixed order of quadrature to evaluate the element integrals. For the nearly singular integrals, when the source and field elements are collocated, we use a higher-order Gauss-Legendre quadrature. And low order quadrature when the source and field elements are far apart. The centerline of the beams is discretized and interpolated by third-order piecewise polynomials, and the hydrodynamic boundary force is decomposed into first-order linear B-spline as the basis function. We will provide a complete procedure to apply this method with two

test cases of passive microcantilever array undergoes an externally imposed shear flow and also actively-driven cantilevers in stagnant fluids.

The thesis is organized as follows: Chapter 2 presents the reader with a quick overview of the equation of motions of fluid-beam interactions and constitutive relations. It then followed with an overview of the spatial, temporal discretization, and non-dimensionalization of the coupled system. Chapter 3 focuses on a few essential microhydrodynamics theory such as the fundamental solutions in a free and bounded domain, which lead to the reformulation of the Stokes equation into boundary integral equations. The reader can skip chapter 3 first and come back later when necessary. In chapter 4, we discretized and solved the boundary integral equation using the Galerkin boundary element method with a step-by-step numerical procedure. In chapter 5, we provide simulation results and demonstrated numerical convergence and accuracy with two test examples: an array of passive microcantilever undergoes an externally imposed shear flow and actively-driven cantilevers in stagnant fluids. In our simulation results, we found a stagnant layer region formed surrounding the lower half of the actively-driven cantilever at the vicinity of the wall, in contrast to the increased mixing and transport properties at the upper half region of the cantilevers.

Chapter 2 Equations of motion

The purpose of this chapter is to present a brief overview of the mathematical models of the immersed microstructures. First, we will introduce the system of equations to be solved in this thesis. We will then provide the non-dimensionalization procedure, which is crucial to organize physical parameters in simulations and to make efficient simulations strategy. We then provide a brief overview of spatial and temporal discretization in matrix form and a summary of the overall algorithms.

2.1 Overview of equations of motion

In this thesis, we solve the following fluid-structure interactions equations system, where the bold letters represent vector quantities in a three-dimensional Cartesian coordinate of x, y, z.

Unknowns: $\mathbf{X}, \mathbf{U}, \mathbf{u}, p$

Equation of motion (EOM):

$$\rho \frac{\partial^2 \mathbf{X}}{\partial t^2} = \mathbf{F}^{elastic}(\mathbf{X}) + \mathbf{F}^{hydro}(\mathbf{U}), \quad (1)$$

Constitutive relations:

Solids

{

$$\mathbf{F}^{elastic}(\mathbf{X}) = -EI \frac{\partial^4 \mathbf{X}}{\partial s^4} + b \frac{\partial^2 \mathbf{X}}{\partial s^2}, \quad (2)$$

$$BCs: \mathbf{X}, \frac{\partial \mathbf{X}}{\partial s}, \frac{\partial^2 \mathbf{X}}{\partial s^2}, \frac{\partial^3 \mathbf{X}}{\partial s^3}$$

Fluids

{

$$-\mu \nabla^2 \mathbf{u} + \nabla p = \mathbf{0}$$

$$\nabla \cdot \mathbf{u} = 0$$

$$BCs: \mathbf{u} = \mathbf{U} - \mathbf{u}_{bg}, \quad \mathbf{F}^{hydro} = \int_S \sigma_{ij} n_j dS$$

Where ρ is the density of the beam in mass per unit length, E is the young's modulus, I is the second moments of areas with circular cross-sectional areas formula ($I = \frac{\pi}{4}r^2$), EI together is also known as bending rigidity, b is tension coefficient due to stretching, and s is the arch length representing the material points of the beam, and μ is the dynamic viscosity of the fluids in $Pa \cdot s$, and \mathbf{u}_{bg} is the externally imposed background fluids velocity.

The equation of motion (1) of the beams is governed by Newton's second law, which states that force equals the product of mass and acceleration. Motion, such as acceleration, is a kinematic variable, but forces are dynamics. To provide closure, we must represent forces from constitutive relation as kinematic relations to position and velocity. The fundamental difference between the constitutive relations of solids and liquid is that force is proportional to strain in the solid, and proportional to strain rate in the fluid. The internal elastic forces, $\mathbf{F}^{elastic}(\mathbf{X})$, come from the deformation of the beams due to bending, \mathbf{X}_{SSSS} , and stretching term, \mathbf{X}_{SS} , in (2).

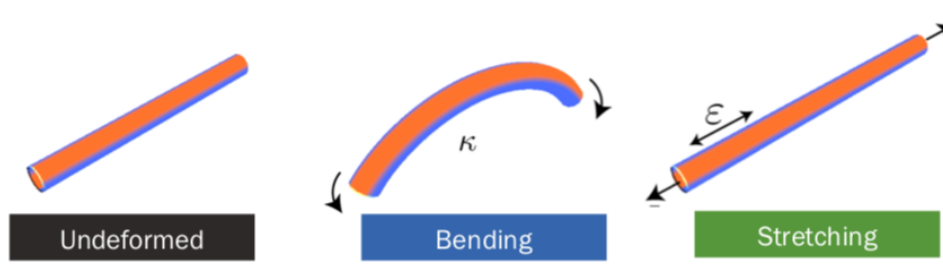


Figure 1 Deformation of the beams due to bending and stretching [11] [12]

The hydrodynamic drag (3) comes from the viscosity in the fluids to be computed as an integral of the fluid stress tensors over the beam boundary. One common approach would require volumetric discretization of the fluid domain to solve for the Stokes equation to satisfy no-slip boundary condition and integrate the fluid stress tensor over the solid boundary numerically.

However, such volumetric discretization methods are not efficient, and would require significant computational time, and introduced a substantial degree of freedom in the equations. Our focus in this thesis is to reformulate the Stokes equation into and solve for a boundary integral relationship between the boundary velocities, \mathbf{U} , and the hydrodynamic traction force, \mathbf{F}^{hydro} . There must exist such a linear relation between \mathbf{U} and \mathbf{F}^{hydro} since the Stokes equations (3) are linear. Let's just first assumed that the relation exists and can be encapsulated into a linear operator \mathcal{L} which is only a function of the time-evolving geometry of the microstructural boundaries.

$$\mathbf{F}^{hydro} = -\mu\mathcal{L}\mathbf{U} \quad (4)$$

Many famous analytical solutions exist for such direct relation when the boundaries are rigid, and geometries are simple. For example, the famous ‘‘Stokes law’’ states that a single sphere of radius, r , traveling with a velocity \mathbf{U} immersed in fluids with viscosity, μ , would experience a drag force \mathbf{F}^{hydro} :

$$\mathbf{F}^{hydro} = -6\pi\mu r\mathbf{U} \quad (5)$$

The boundary integral reformulation of Stokes equations is at heart of this linear relationship between fluids drag forces exerted due to body motions and vice versa. We will introduce in chapter 3 for the formulation of such relation, and discuss its detailed numerical discretization procedure in chapter 4 using the boundary element method.

2.2 Nondimensionalization

We can rewrite EOM (1) explicitly with the constitutive relations of Euler-Bernoulli beams and the Stokes flow boundary integral operator \mathcal{L} :

$$\rho \frac{\partial^2 \mathbf{X}}{\partial t^2} = (-EI \mathbf{X}_{ssss} + b \mathbf{X}_{ss}) - \mu \mathcal{L}(\mathbf{U} - \mathbf{u}_{bg}), \quad (6)$$

Each variable can be non-dimensionalised as the following:

$$\mathbf{X}^* = \frac{\mathbf{X}}{L}, \quad s^* = \frac{s}{L}, \quad t^* = \frac{t}{T_1}, \quad \mathbf{U}^* = \frac{\mathbf{U}}{L/T_1}, \quad \mathbf{u}_{bg}^* = \frac{\mathbf{u}_{bg}}{L/T_2} \quad (7)$$

After substituting the characteristic scales into equation (6), and assume $b \cong EI$, we have:

$$\frac{\rho L}{T_1^2} \frac{\partial^2 \mathbf{X}^*}{\partial t^{*2}} = \frac{EI}{L^3} (-\mathbf{X}^*_{ssss} + \mathbf{X}^*_{ss}) - \mu L \left(\frac{1}{T_1} \mathcal{L} \mathbf{U}^* - \frac{1}{T_2} \mathcal{L} \mathbf{u}_{bg}^* \right), \quad (8)$$

The coefficients in each term of the above have the following unit, and we can see that the units and dimensions in the equation matchup:

$$\left[\frac{\rho L}{T_1^2} \right] = \frac{kg}{m} \frac{m}{s^2} = \frac{kg}{s^2}, \quad \left[\frac{EI}{L^3} \right] = \frac{\frac{N}{m^2} m^4}{m^3} = \frac{kg}{s^2}, \quad \left[\frac{\mu L}{T} \right] = Pa \cdot s \frac{m}{s} = \frac{kg}{s^2} \quad (9)$$

In our applications, we assume that the beam inertia is significant in the EOM and is on the order of 1. Divide both sides of (8) by $\frac{\rho L}{T_1^2}$, and we have the following dimensionless equation :

$$\frac{\partial^2 \mathbf{X}^*}{\partial t^{*2}} = \frac{EIT_1^2}{\rho L^4} (-\mathbf{X}^*_{ssss} + \mathbf{X}^*_{ss}) - \frac{\mu}{\rho} \left(T_1 \mathcal{L} \mathbf{U}^* - \frac{T_1^2}{T_2} \mathcal{L} \mathbf{u}_{bg}^* \right) \quad (10)$$

The characteristic time scale depends on the applications of the problems. We can set the time scale, T_1 , to match up by the elasticity term with an order of 1, and time scale, T_2 , was a given quantity of the externally imposed flow strength, λ .

$$T_1 = \sqrt{\frac{\rho L^4}{EI}}, \quad T_2 = \frac{1}{\lambda} \quad (11)$$

After substituting the characteristic time scales from the elastic relaxation and imposed flow into (10), we obtained the final dimensionless equation parameterized by two parameters of C_1 and C_2 , which are ready for numerical discretization.

$$\frac{\partial^2 \mathbf{X}^*}{\partial t^{*2}} = (-\mathbf{X}^*_{ssss^*} + \mathbf{X}^*_{ss^*}) - C_1 \mathcal{L}\mathbf{U}^* + C_2 \mathcal{L}\mathbf{u}_{bg}^* \quad (12)$$

$$C_1 = \sqrt{\frac{\mu^2 L^4}{\rho EI}}, \quad C_2 = \frac{\lambda \mu L^4}{EI}$$

In the case of no external flow where $\lambda = 0$, we have the following equation characterized by a single parameter C_1 .

$$\frac{\partial^2 \mathbf{X}^*}{\partial t^{*2}} = (-\mathbf{X}^*_{ssss^*} + \mathbf{X}^*_{ss^*}) - C_1 \mathcal{L}\mathbf{U}^* \quad (13)$$

$$C_1 = \sqrt{\frac{\mu^2 L^4}{\rho EI}}$$

2.3 Spatial discretization

For the fluids, suppose that we have discretized the boundary integral operator in (4) into the matrix form of \mathbf{R} which also absorbs the dimensionless parameters and the negative signs. We have the following discretized relation for fluid mechanics

$$\mathbf{f}_n^{hydro} = \mathbf{R}\mathbf{u}_n \quad (14)$$

The Euler-Bernoulli beam equation (2) can be solved by a variety of spatial discretization methods such as finite element (FE), finite-volume (FV), finite-difference (FD). For simplicity of implementations, it is discretized here using standard finite difference method with boundary conditions applied at both ends. Once we discretized them in the FD matrix form, they could then be easily solved using linear algebra routine.

$$\mathbf{f}_n^{elastic} = \mathbf{A}\mathbf{x}_n + \mathbf{b}_n \quad (15)$$

where \mathbf{A} is the matrix form of the FD stencil for the fourth and second-order derivative operators, and \mathbf{b}_n is the boundary conditions applied at both ends of the beam. In our case, we set one end to be fixed and the other to be stress-free. It was worth commenting that, \mathbf{A} , the elastic matrix from the finite-difference discretization, has a tightly-banded sparsity diagonal structure, but, \mathbf{R} , the hydrodynamic matrix developed in chapter 4, is a full dense matrix.

2.4 Temporal discretization

We can then substitute the spatially discretized elastic and hydrodynamic functions into the EOM (1) leading to a system of ordinary differential equations:

$$\frac{d^2 \mathbf{x}_n}{dt^2} = (\mathbf{A}\mathbf{x}_n + \mathbf{b}_n) + \mathbf{R}\mathbf{u}_n \quad (16)$$

The temporal discretization is implemented by a semi-implicit Euler method, where the elastic matrix is solved implicitly in time at $(t + 1)$ and hydrodynamic matrix explicitly at (t) :

$$\begin{aligned}\mathbf{x}_n^{(t+1)} &= \mathbf{x}_n^{(t)} + \mathbf{u}_n^{(t+1)}dt \\ \mathbf{u}_n^{(t+1)} &= \mathbf{u}_n^{(t)} + (\mathbf{A}\mathbf{x}_n^{(t+1)} + \mathbf{b}_n + \mathbf{R}^{(t)}\mathbf{u}_n^{(t)})dt\end{aligned}\tag{17}$$

The above equation can be rewritten as:

$$\mathbf{x}_n^{(t+1)} = (\mathbf{I} - \mathbf{A}dt)^{-1} (\mathbf{x}_n^{(t)} + \mathbf{u}_n^{(t)}dt + (\mathbf{b}_n + \mathbf{R}^{(t)}\mathbf{u}_n^{(t)})dt^2)\tag{18}$$

$$\mathbf{u}_n^{(t+1)} = \mathbf{u}_n^{(t)} + (\mathbf{A}\mathbf{x}_n^{(t+1)} + \mathbf{b}_n + \mathbf{R}^{(t)}\mathbf{u}_n^{(t)})dt\tag{19}$$

We also provide the formulation for beams with negligible inertia in matrix form, and please refer to *Appendix A* for more details.

2.5 Algorithms Overview

Algorithm overview

1. **Require:** initial position and velocity of beams, and interpolations
 2. **While** simulating **do**
 3. compute hydrodynamic forces on beam through Boundary element method
 4. compute elastic forces on beam through Finite difference method
 5. Integrating equations of motion in time semi-explicitly (18) and (19)
 6. compute new interpolation of beam
 7. **end while**
-

Chapter 3 Microhydrodynamics

In chapter 3, we summarised the necessary theoretical foundations [13–16] for slow, inertialess, and very viscous flow leading to the boundary integral reformulation of Stokes equation around slender bodies. We first provide a brief overview of the principle of mass and momentum conservation in continuum media and constitutive relation of the general Newtonian fluid. The Stokes equations are then introduced as a result of the momentum equation approaching zero Reynold number asymptotic limit. After establishing the governing equations, we proceed with presenting their Green’s function in free space and introduced the modified solution bounded by a wall. The flow field created by a surface distribution of forces on a continuum body can then be represented by boundary integral equations. In addition, due to the small aspect ratio of the slender body, the surface integrals can be approximated as a line integral of fundamental solutions along the centerline. We end this chapter with a brief discussion on the regularized Stokeslet method to provide a simple numerical fix on the singularity of Stokeslet when the field point is evaluated at the source.

3.1. Principles of mass and momentum conservation

The conservation equations of mass and momentum of any continuum can be written as the following in an inertial frame of references (ignore Coriolis and centrifugal accelerations) where ρ is the density, u_i the velocity, σ_{ij} the stress tensors due to surface forces and g_i the body forces.

Rate of change of mass = 0

$$\frac{\partial \rho}{\partial t} + \frac{\partial \rho u_i}{\partial x_i} = 0 \quad (20)$$

Rate of change of momentum = sum of applied forces (surface forces+ body forces)

$$\left(\frac{\partial \rho u_i}{\partial t} + \frac{\partial \rho u_i u_j}{\partial x_j} \right) = \frac{\partial \sigma_{ij}}{\partial x_i} + \rho g_i \quad (21)$$

A Newtonian fluid is a phenomenological model with a constant dissipation rate (i.e., viscosity), and a fixed tensorial structure, where μ is the dynamic viscosity [Pa s], μ_b is the bulk viscosity, and p is the pressure.

$$\sigma_{ij} = -p \delta_{ij} + \mu \left(\frac{\partial u_i}{\partial x_j} + \frac{\partial u_j}{\partial x_i} \right) + \left(\mu_b - \frac{2}{3} \mu \right) \delta_{ij} \left(\frac{\partial u_k}{\partial x_k} \right) \quad (22)$$

In the case of constant density and incompressible fluids ($\frac{\partial u_k}{\partial x_k} = 0$), the generalized constitutive relation above can be simplified into the following:

$$\sigma_{ij} = -\delta_{ij} p + \mu \left(\frac{\partial u_i}{\partial x_j} + \frac{\partial u_j}{\partial x_i} \right) \quad (23)$$

And the general mass (20) and momentum (21) conservation equation could be reduced into the famous incompressible Navier-Stokes equations in the following dimensionless form parametrized by Reynold number ($Re = \frac{\rho UL}{\mu}$):

$$\frac{\partial u_i^*}{\partial x_i^*} = 0 \quad (24)$$

$$Re \left(\frac{\partial u_i^*}{\partial t} + u_j^* \frac{\partial u_i^*}{\partial x_j^*} \right) = -\frac{\partial P^*}{\partial x_i^*} + \frac{\partial^2 u_i^*}{\partial x_j^{*2}} \quad (25)$$

When Reynold number is approaching zero asymptotic limits ($Re \ll 1$), we can ignore the momentum on the LHS of (25) and obtained the linearized Stokes equation. On the contrary

to Navier-Stokes equations, Stokes flow is linear, time-symmetric, unique in its solutions, and it also leads to minimum energy dissipation compared to the solution from the full Navier-Stokes under the same boundary conditions. For further information on these unique properties, please refer to excellent materials [13–16] for details. However, it is essential to keep in mind that physically Re could never be zero, even at the microscale. When significant acceleration happens, the fluids can “jump” out of zero Reynold number regime, where the inertia becomes essential, such as microscale acoustic streaming phenomenon. Nevertheless, the Stokes equation is an accurate fluids mechanics model when the Reynold number is well below unity.

$$0 = -\frac{\partial P}{\partial x_i} + \mu \frac{\partial^2 u_i}{\partial x_j^2} = \frac{\partial \sigma_{ij}}{\partial x_i} \quad (26)$$

$$\frac{\partial u_i}{\partial x_i} = 0 \quad (27)$$

3.2. Fundamental solutions of Stokes equation

In this section, we present the famous fundamental solutions of the Stokes flow. Considering a particular flow configuration at x_i as a result of a point force f_i applied at x_i^0 , the singularly forced Stokes equation reads:

$$0 = -\frac{\partial P}{\partial x_i} + \mu \frac{\partial^2 u_i}{\partial x_j^2} + f_i \delta(r) = \frac{\partial \sigma_{ij}}{\partial x_j} + f_i \delta(r) \quad (28)$$

$$\frac{\partial u_i}{\partial x_i} = 0 \quad (29)$$

where $\hat{x}_i = x_i - x_i^0$, $r = \sqrt{\hat{x}_i \hat{x}_i}$, and $\delta(r)$ is a three-dimensional Dirac function and the volume integral took place on arbitrary domain enclosed x_i^0 :

$$\begin{cases} \delta(r) = 0, & \text{for } x_i \neq x_i^0 \\ \delta(r) = \infty, & \text{for } x_i = x_i^0 \end{cases} \quad (30)$$

$$\iiint \delta(x_i - x_i^0) f_i dV(x_i) = f_i \quad (31)$$

The fundamental solutions are basically spatial impulse response of the Stokesian fluid. We can express the free-space solutions due to a point forces in terms of each of their well-known Green's functions: Stokeslet S_{ij} , Stresslet T_{ijk} , and Pressurelet P_j . (See *appendix B* for their derivation).

$$u_i(x_i) = \frac{1}{8\pi\mu} S_{ij}(x_i - x_i^0) f_j, \quad S_{ij}(x_i - x_i^0) = \frac{\delta_{ij}}{r} + \frac{\hat{x}_i \hat{x}_j}{r^3} \quad (32)$$

$$\sigma_{ik}(x_i) = \frac{1}{8\pi} T_{ijk}(x_i - x_i^0) f_j, \quad T_{ijk}(x_i - x_i^0) = -6 \frac{\hat{x}_i \hat{x}_j \hat{x}_k}{r^5} \quad (33)$$

$$p(x_i) = \frac{1}{8\pi} P_j(x_i - x_i^0) f_j, \quad P_j(x_i - x_i^0) = 2 \frac{\hat{x}_j}{r^3} \quad (34)$$

The Stokeslet (32), a second-order tensor in 3D, encapsulate a linear mobility relation between an applied point force and velocity field in the fluids, which could be written explicitly as the following:

$$\begin{pmatrix} u_x \\ u_y \\ u_z \end{pmatrix} = \frac{1}{8\pi\mu} \begin{pmatrix} S_{xx} & S_{xy} & S_{xz} \\ S_{yx} & S_{yy} & S_{yz} \\ S_{zx} & S_{zy} & S_{zz} \end{pmatrix} \begin{pmatrix} f_x \\ f_y \\ f_z \end{pmatrix} \quad (35)$$

$$\begin{pmatrix} u_x \\ u_y \\ u_z \end{pmatrix} = \frac{1}{8\pi\mu} \begin{pmatrix} \frac{1}{r} + \frac{(x-x^0)(x-x^0)}{r^3} & \frac{(x-x^0)(y-y^0)}{r^3} & \frac{(x-x^0)(z-z^0)}{r^3} \\ \frac{(y-y^0)(x-x^0)}{r^3} & \frac{1}{r} + \frac{(y-y^0)(y-y^0)}{r^3} & \frac{(y-y^0)(z-z^0)}{r^3} \\ \frac{(z-z^0)(x-x^0)}{r^3} & \frac{(z-z^0)(y-y^0)}{r^3} & \frac{1}{r} + \frac{(z-z^0)(z-z^0)}{r^3} \end{pmatrix} \begin{pmatrix} f_x \\ f_y \\ f_z \end{pmatrix} \quad (36)$$

When the flow is bounded, the presence of the wall can be incorporated analytically into the Green's function using the method of images. In the case of satisfying no penetration condition, one can simply place a Stokeslet of equal strength at the mirrored side of the plane due to symmetry.

$$G_{ij}^{wall} = S_{ij}(x_i, x_i^0) + \Delta S_{ij}(x_i, \widetilde{x}_i^0) \quad (37)$$

where $\Delta = 1 - 2\delta_{j3}$ is a reflection operator in the direction that's normal to the wall, z-axis in our case. Δ has a minus sign for $j = 3$ (z-direction), and a plus sign for $j = 1, 2$ (x, y directions). However, to satisfy no-slip boundary condition, the construction of modified Green's function is a bit more complicated, and we will not be re-deriving it in here. Blake [17] (1971) initially showed through Fourier transform method that the velocity green's function bounded by a plane wall can be constructed as a finite set of singularities solutions: Stokeslet, mirrored Stokeslet, a point-source dipole and Stokeslet dipole, where \widetilde{x}_i^0 is the imaged location of x_i^0 , and $h = x_3^0 - w$ is the normal distance to the wall.

$$G_{ij}^{wall}(x_i, x_i^0) = S_{ij}(x_i, x_i^0) - S_{ij}(x_i, \widetilde{x}_i^0) + 2h^2\Delta \frac{\partial}{\partial x_j} \left(\frac{x_i - \widetilde{x}_i^0}{|x_i - \widetilde{x}_i^0|^3} \right) - 2h\Delta \frac{\partial S_{i3}(x_i, \widetilde{x}_i^0)}{\partial x_j} \quad (38)$$

Although the Green's function is modified, the outer structure of the velocity-force relation does not change, $u_i(x_i) = \frac{1}{8\pi\mu} G_{ij}^{wall} f_j$. This encapsulation of modified Green's function can be a very powerful one in numerical implementation. Please see *appendix C* for the definition of source dipole, Stokeslet dipole, and higher multipole generalization of the green's function.

3.3 Boundary integral equation

Up to this point, the velocity green's function establishes a mobility relation between a point force and the velocity field in the fluid. This could be generalized into a continuum body where the surface distribution of forces would create a superposition of flow field due to individual forces density $f_i(\mathbf{x})$. The boundary integral equation generalized such a relation by exploring the linearity and reciprocal relation in Stokes equation: (See its derivation from reciprocal relation in *appendix D*)

$$u_j(\mathbf{x}^0) = -\frac{1}{8\pi\mu} \iint_S S_{ji}(\mathbf{x}^0, \mathbf{x}) f_i(\mathbf{x}) dS(\mathbf{x}) \quad (39)$$

Also, the surface integrals of a long slender object could be approximated using non-local slender body theory (SBT), an asymptotic method. The core idea in SBT is that the surface integral around the loop of the centerline can be shrunk into a line integral along the centerline using multipoles expansion technique. Consider a tube, its surface location, x_i , can be parametrized by the following, where “ \mathbf{r} ” is the centerline location, “ \mathbf{b} ” is binormal and “ \mathbf{n} ” is normal direction, and “ a ” is the radius of the tube:

$$x_i = \mathbf{r}(s, t) + a\hat{\boldsymbol{\theta}}, \quad \hat{\boldsymbol{\theta}} = a(\cos \theta \mathbf{n} + \sin \theta \mathbf{b}) \quad (40)$$

The surface integral of the tube is the following:

$$u_j(\mathbf{x}^0) = -\frac{1}{8\pi\mu} \int_l \int_{\theta} S_{ij}(\mathbf{x}^0, \mathbf{r} + a\hat{\boldsymbol{\theta}}) f_i(\mathbf{r} + a\hat{\boldsymbol{\theta}}) d\theta dl(\mathbf{r}) \quad (41)$$

We can first non-dimensionalise the surface position x_i by the length of the tube, L :

$$\frac{x_i}{L} = \frac{\mathbf{r}(s, t)}{L} + \frac{a}{L} \widehat{\boldsymbol{\theta}} \quad (42)$$

$$x_i^* = \mathbf{r}^* + \epsilon \widehat{\boldsymbol{\theta}} \quad (43)$$

And do a Taylor series expansions of the Stokeslet around centerline location \mathbf{r}^* ,

$$S_{ij}(x_i^0, \mathbf{r}^* + \epsilon \widehat{\boldsymbol{\theta}}) = S_{ij}(x_i^0, \mathbf{r}^*) - \epsilon \widehat{\boldsymbol{\theta}} \frac{\partial S_{ij}(x_i^0, \mathbf{r}^*)}{\partial x_k} - \frac{1}{2} \epsilon^2 \widehat{\boldsymbol{\theta}} \widehat{\boldsymbol{\theta}} \frac{\partial^2 S_{ij}(x_i^0, \mathbf{r}^*)}{\partial x_m \partial x_k} + H.O.T \quad (44)$$

When the aspect ratio ϵ is a very small number, we can retain the zeroth-order term and discard the rest in (44). Therefore, the dependence of the integral on cross-sectional surface areas of the tube is eliminated, since $S_{ij}(x_i^0, \mathbf{r}^*)$ depend only on the centerline position of the body, \mathbf{r}^* . Substitute it back to the surface integrals equation (41), we get:

$$u_i(\mathbf{x}^0) = -\frac{1}{8\pi\mu} \int_l S_{ij}(\mathbf{x}^0, \mathbf{r}) \int_{\theta} f_i(\mathbf{r} + a\widehat{\boldsymbol{\theta}}) d\theta dl(\mathbf{r}) \quad (45)$$

Which can then be rewritten into a form in terms of the integrated forces along the cross-sectional loop of the body, $f_j^*(\mathbf{r}) = \int_{\theta} f_j(\mathbf{r} + a\widehat{\boldsymbol{\theta}}) d\theta$

$$u_i(\mathbf{x}^0) \cong -\frac{1}{8\pi\mu} \int_l S_{ij}(\mathbf{x}^0, \mathbf{r}) f_j^*(\mathbf{r}) dl(\mathbf{r}) \quad (46)$$

Where $dl(\mathbf{r})$ represent the differential of the line integral as a function of centerline position, \mathbf{r} . The velocity field can, therefore, be approximated as driven by a line integral of Stokeslet rather than taking consideration of the surface of the tube. The key idea is that flow disturbance created by a slender body surface is equivalent to applied point forces distributed over the centerline of the body.

3.4 Singularity regularization

The Green's functions presented so far are singular when evaluating velocity (field) and force (source) at the same point. The regularized Stokeslet method developed by Cortez [18] can be used to regularize the singularity of the solutions. The main advantage of such an approach is that the regularized solutions remain regular at the point of applied forces, and collocation can be performed at such point with standard quadrature without advanced adaptive numerical quadrature or semi-analytical quadrature rules. The reader can refer to their paper for more details, and we provide a very brief summary of the method here. The essential idea in the regularized Stokeslet method is to rederive the regularized Green's function through forcing the Stokes equation with a regularized delta function, ϕ_ϵ , with finite parameter ϵ , in place of singular Dirac delta, $\delta(r)$. It was also proven by Cortez to also satisfy the reciprocal relation of the Stokes equations. Therefore, it can be formulated into the boundary integral equations. In the limit of ϵ approaching zero, both the delta function and the Stokeslet can be recovered.

$$\phi_\epsilon(\mathbf{x} - \mathbf{x}_0) = \frac{15\epsilon^4}{8\pi(r^2 + \epsilon^4)^{7/2}} \quad (47)$$

$$-\mu\nabla^2\mathbf{u} + \nabla p = \mathbf{f}\phi_\epsilon(\mathbf{x} - \mathbf{x}_0) \quad (48)$$

$$\nabla \cdot \mathbf{u} = 0$$

Repeat the solution procedure in *appendix B* with a regularized delta function, ϕ_ϵ , in place of δ , and the expression for the regularized Stokeslet could be obtained:

$$S_{ij}^\epsilon = \frac{\delta_{ij}(r^2 + 2\epsilon^2)}{r_\epsilon^3} + \frac{\hat{x}_i\hat{x}_j}{r_\epsilon^3}, \quad r_\epsilon = \sqrt{r^2 + \epsilon^2} \quad (49)$$

They also developed the numerically regularized solution [19] for the flow bounded by a wall based on the analytical solutions developed by Blake [17] (1971), which have been later used to study flagella driven flow by Smith [8].

Chapter 4 Boundary Element method

Our main task in this chapter is to find an efficient and accurate way to discretize and solve for the following boundary integral reformulation of the 3D Stokes flow around slender bodies:

$$u_i(\mathbf{x}) = -\frac{1}{8\pi\mu} \int_l S_{ij}(\mathbf{x}, \mathbf{r}) f_j(\mathbf{r}) dl(\mathbf{r}) \quad (50)$$

If either $u_i(\mathbf{x})$ or $f_j(\mathbf{r})$ is given, the above equation can be solved for the other unknown.

In our case, we are given the boundary velocities, $u_i(\mathbf{r}^0)$, and solve for the unknown hydrodynamic traction forces, $f_j(\mathbf{r})$, where \mathbf{r} and \mathbf{r}^0 are the position of the centerlines of the slender body.

$$u_i(\mathbf{r}^0) = -\frac{1}{8\pi\mu} \int_l S_{ij}(\mathbf{r}^0, \mathbf{r}) f_j(\mathbf{r}) dl(\mathbf{r}) \quad (51)$$

Once the boundary forces, $f_j(\mathbf{r})$, are calculated from (51), the boundary integral equation (50) can be used again to compute the velocities, $u_i(\mathbf{x})$, directly at any desired location, \mathbf{x} , in the surrounding 3D fluids domain at the post-processing stages.

In this chapter, we will first give an overview of two different approaches to numerically discretizing the integral equation (51). One straightforward approach is the Nystrom method through directly approximating the integral equation using numerical quadrature at the collocation points. Then we will present issues of such an approach. After that, we will introduce the alternative boundary element discretization approach through the method of weighted residuals with emphasis mainly on the Galerkin method. After that, we provide implementation

details on how to interpolate the domain by using piecewise polynomials and perform numerical integration over each piecewise polynomials subdomains. This chapter will end with a summary of the three-level discretization of the hydrodynamic mobility matrix due to a point force, due to a continuous body, and due to N body interaction. (Note that i, j are the indexes in Einstein notation ($i = j = [x, y, z]$). m, n are the discretisation indexes.)

4.1 Nystrom method

One typical approach for solving the integral equation is to directly discretize the whole integral using numerical quadrature such as Nystrom method where quadrature point is equal to the collocation point of the variables, and w_n is some quadrature weights:

$$u_i(\mathbf{r}^0_m) = \sum_{n=1}^N S_{ij}(\mathbf{r}^0_m, \mathbf{r}_n) f_j(\mathbf{r}_n), \quad f_j(\mathbf{r}_n) = -\frac{w_n}{8\pi\mu} f_{j_n} \quad (52)$$

$S_{ij}(\mathbf{r}^0_m, \mathbf{r}_n)$ has the following matrix form where each submatrix, such as $S_{x_mx_n}$, is indexed by $\mathbf{m} \otimes \mathbf{n}$, the dyadic product of the discretization indexes \mathbf{m} and \mathbf{n} :

$$\begin{pmatrix} u_{x_m} \\ u_{y_m} \\ u_{z_m} \end{pmatrix} = \begin{pmatrix} S_{x_mx_n} & S_{x_my_n} & S_{x_mz_n} \\ S_{y_mx_n} & S_{y_my_n} & S_{y_mz_n} \\ S_{z_mx_n} & S_{z_my_n} & S_{z_mz_n} \end{pmatrix} \begin{pmatrix} f_{x_n} \\ f_{y_n} \\ f_{z_n} \end{pmatrix} \quad (53)$$

We can solve for $f_j(\mathbf{r}_n)$ given by $u_i(\mathbf{r}^0_m)$, or vice versa. However, in this approach, the discretization of variables and integral is implicitly coupled. For example, if one wants to reduce the variables discretization in the integral equation, the quadrature discretization for integrals also has to be reduced. And if more quadrature points are desired for the integral, the variables discretization will also have to be increased, which will introduce unnecessary degrees of

freedom in the discretized integral equation. Boundary element method (BEM) could alleviate this issue by decoupling the variables discretization and numerical quadrature.

4.2 Weighted residual method

Boundary element methods (BEM) works by first decomposing the variables, hydrodynamic boundary forces, and boundary velocities, into locally supported basis functions (ansatz), $\boldsymbol{\phi}_n(s)$, where s and s^0 are the arch length parametrization of the domain, and \mathbf{f}_n and \mathbf{u}_n are the coefficients of the basis function:

$$f_j(\mathbf{r}) = \sum_{n=1}^N \mathbf{f}_n \boldsymbol{\phi}_n(s), \quad u_i(\mathbf{r}^0) = \sum_{n=1}^N \mathbf{u}_n \boldsymbol{\phi}_n(s^0) \quad (54)$$

$$\boldsymbol{\phi}_n(s) = [\phi_n^x(s), \phi_n^y(s), \phi_n^z(s)] \quad (55)$$

$$\mathbf{f}_n = [f_n^x, f_n^y, f_n^z] \quad (56)$$

$$\mathbf{u}_n = [u_n^x, u_n^y, u_n^z] \quad (57)$$

The first order B-splines are used as the basis functions for both forces and velocities, which are locally supported over two elements and defined as the following:

$$\phi_n(s) = \begin{cases} s, & s_{n-1} \leq s \leq s_n \\ -s, & s_n \leq s \leq s_{n+1} \\ 0, & \text{elsewhere} \end{cases} \quad (58)$$

The residual function can be obtained by rearranging terms in boundary integral equation (51) into the following:

$$R(\mathbf{r}^0) = u_i(\mathbf{r}^0) + \frac{1}{8\pi\mu} \int_l S_{ij}(\mathbf{r}^0, \mathbf{r}) f_j(\mathbf{r}) dl(\mathbf{r}) \quad (59)$$

The weighted average of the residual functions are enforced to be zero, where $\boldsymbol{\varphi}_m(s)$ is the weighting function:

$$\int_l \boldsymbol{\varphi}_m(s^0) R(\mathbf{r}^0) dl(\mathbf{r}^0) = 0 \quad (60)$$

The essential idea in the method of weighted residual is that by varying the coefficients of the basis functions, \mathbf{u}_n and \mathbf{f}_n , we can satisfy the constraints posed by the weighted residual equations above in (60). In our case, we were given coefficients of boundary velocity, \mathbf{u}_n , to determine the unknown coefficients of, \mathbf{f}_n . And we can rewrite the method of weighted residual (MWR) explicitly as:

$$\int_l \sum_{n=1}^N \mathbf{u}_n \boldsymbol{\phi}_n(s^0) \boldsymbol{\varphi}_m(s^0) dl(\mathbf{r}^0) = -\frac{1}{8\pi\mu} \sum_{n=1}^N \mathbf{f}_n \int_l \int_l S_{ij}(\mathbf{r}^0, \mathbf{r}) \boldsymbol{\phi}_n(s) \boldsymbol{\varphi}_m(s^0) dl(\mathbf{r}) dl(\mathbf{r}^0) \quad (61)$$

There are a variety of choices in weighting functions resulting in different types of equation constraints. The notable ones are collocation, Galerkin, and spectral method.

Collocation method:

$$\boldsymbol{\varphi}_m(s) = \boldsymbol{\delta}(s_c - s) \quad (62)$$

Galerkin method:

$$\boldsymbol{\varphi}_m(s) = \boldsymbol{\phi}_m(s) \quad (63)$$

In the Galerkin method, the weighting function, $\boldsymbol{\varphi}_m(s)$, is the same as the basis function $\boldsymbol{\phi}_m(s)$, and therefore the equation is enforced at elements spanned by the locally supported

basis functions. The following is the discretized equation from Galerkin method by projecting the boundary integral equation onto the m^{th} basis function $\boldsymbol{\phi}_m$:

$$\sum_{n=1}^N \mathbf{u}_n \int \boldsymbol{\phi}_n(s^0) \boldsymbol{\phi}_m(s^0) dl(\mathbf{r}^0) = -\frac{1}{8\pi\mu} \sum_{n=1}^N \mathbf{f}_n \int \int S_{ij}(\mathbf{r}^0, \mathbf{r}) \boldsymbol{\phi}_n(s) \boldsymbol{\phi}_m(s^0) dl(\mathbf{r}) dl(\mathbf{r}^0) \quad (64)$$

We can rewrite the Galerkin equation (64) explicitly in terms of coefficients of the basis function, \mathbf{f}_n and \mathbf{u}_n , where m and n are discretization indexes of the matrix due to m^{th} or n^{th} basis function

$$\sum_{n=1}^N \mathbf{E}_{mn} \mathbf{u}_n = -\frac{1}{8\pi\mu} \sum_{n=1}^N \mathbf{f}_n \mathbf{S}_{mn} \quad (65)$$

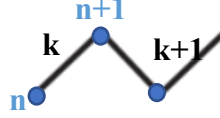
$$\mathbf{E}_{mn} = \int \boldsymbol{\phi}_n(s^0) \boldsymbol{\phi}_m(s^0) dl(\mathbf{r}^0), \quad \mathbf{S}_{mn} = \int \int S_{ij}(\mathbf{r}^0, \mathbf{r}) \boldsymbol{\phi}_n(s) \boldsymbol{\phi}_m(s^0) dl(\mathbf{r}) dl(\mathbf{r}^0) \quad (66)$$

The above equation can be reorganized into the matrix format and solved by standard linear algebra routines as the following:

$$\mathbf{E}\mathbf{u} = -\frac{1}{8\pi\mu} \mathbf{S}\mathbf{f} \quad (67)$$

4.3 Geometric interpolations

From our discretized equation of motion, we only have discrete nodal values of the domains. But the boundary element method would require local integration over the subdomain between nodal values. Therefore, we require interpolation to provide a continuous subdomain for evaluating the integral in \mathbf{E}_{mn} and \mathbf{S}_{mn} . For this section, I implemented the 3rd order piecewise polynomials interpolation method [10]. Please see *Appendix E* for the formulation and implementation details. In the end, the following analytical expressions of the 3rd order piecewise polynomials can be obtained from the interpolations process:



$$\mathbf{r}_k(s) = [x_k(s), y_k(s), z_k(s)] \quad (68)$$

$$\begin{aligned} x_k(s) &= a_k(s - s_n)^3 + b_k(s - s_n)^2 + c_k(s - s_n) + x_n^G \\ y_k(s) &= a'_k(s - s_n)^3 + b'_k(s - s_n)^2 + c'_k(s - s_n) + y_n^G \\ z_k(s) &= a''_k(s - s_n)^3 + b''_k(s - s_n)^2 + c''_k(s - s_n) + z_n^G \end{aligned} \quad (69)$$

where a,b,c are coefficients obtained from the interpolation. The differentials of the line integrals have the following parametrized form of the piecewise polynomials:

$$dl(\mathbf{r}_k) = \sqrt{dx^2 + dy^2 + dz^2} = h_k(s)ds \quad (70)$$

$$\begin{aligned} h_k(s) &= ([3a_k(s - s_n)^2 + 2b_k(s - s_n) + c_k]^2 \\ &\quad + [3a'_k(s - s_n)^2 + 2b'_k(s - s_n) + c'_k]^2 \\ &\quad + [3a''_k(s - s_n)^2 + 2b''_k(s - s_n) + c''_k]^2)^{\frac{1}{2}} \end{aligned} \quad (71)$$

Also, the arc length, s , can be normalized into ξ for each element so that we can use standard numerical quadrature weight from tabulations. The following formulae provide normalization procedure for converting piecewise arch length from $s_n \leq s \leq s_{n+1}$ into $-1 \leq \xi \leq 1$.

$$s(\xi) = 0.5(s_n + s_{n+1}) + 0.5(s_{n+1} - s_n)\xi \quad (72)$$

$$ds = 0.5(s_{n+1} - s_n)d\xi \quad (73)$$

Now we have a set of relations to map the discrete nodal values into continuous smoothly connected subdomains that are ready for computing the subdomain integrals.

4.4 Numerical integration:

In this section, we provide an example on the procedures of computing the integral numerically over each basis function $\phi_n(s)$:

$$\int_l S_{ij}(\mathbf{r}^0, \mathbf{r}) \phi_n(s) dl(\mathbf{r})$$

Since the first order B spline, ϕ_n , is locally supported by two elements, E_{k-1} E_k , and elsewhere are zero. Therefore, each element has contributions from two non-zero basis functions. The following figure shows the normalized non-zero basis function over one single element, which ξ is the normalized piecewise arch length for each element, ranging $[-1 1]$, and also the non-normalized higher-order B-spline functions.

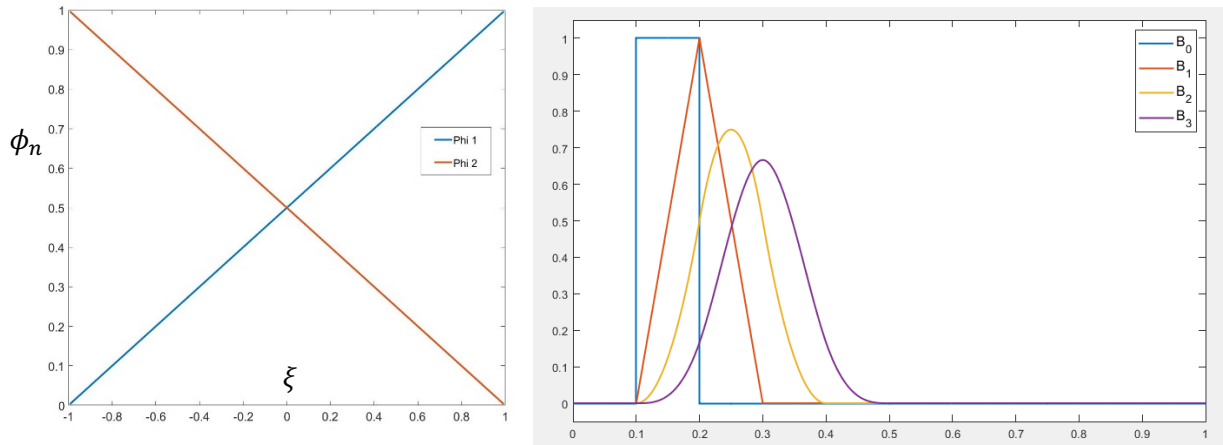


Figure 2 a) two nonzero first-order basis functions over one element. b) Different order of B-spline basis functions

Due to the local supportedness of the basis function, we can simplify the global line integral over n^{th} basis function as following:

$$\int_l S_{ij}(\mathbf{r}^0, \mathbf{r}) \phi_n(s) dl(\mathbf{r}) = \int_{E_{k-1}} S_{ij}(\mathbf{r}^0, \mathbf{r}) \phi_n(s) dl(\mathbf{r}) + \int_{E_k} S_{ij}(\mathbf{r}^0, \mathbf{r}) \phi_n(s) dl(\mathbf{r}) \quad (74)$$

Substituting the piecewise polynomials interpolation for the subdomain of E_{k-1} and E_k :

$$\int_{E_{k-1}} S_{ij}(\mathbf{r}^0, \mathbf{r}_{k-1}(s)) \phi_n(s) dl(\mathbf{r}_{k-1}(s)) + \int_{E_k} S_{ij}(\mathbf{r}^0, \mathbf{r}_k(s)) \phi_n(s) dl(\mathbf{r}_k(s)) \quad (75)$$

And normalizing s with ξ , we obtain the following relation:

$$\int_{-1}^1 [I_{k-1}(\mathbf{r}^0, \xi) + I_k(\mathbf{r}^0, \xi)] d\xi = \int_{-1}^1 I_n(\mathbf{r}^0, \xi) d\xi \quad (76)$$

Where

$$I_k(\mathbf{r}^0, \xi) d\xi = \frac{1}{2}(s_{n+1} - s_n) S_{ij}(\mathbf{r}^0, \mathbf{r}_k(s(\xi))) \boldsymbol{\phi}_n(s(\xi)) h_k(s(\xi)) d\xi \quad (77)$$

$$I_{k-1}(\mathbf{r}^0, \xi) d\xi = \frac{1}{2}(s_n - s_{n-1}) S_{ij}(\mathbf{r}^0, \mathbf{r}_{k-1}(s(\xi))) \boldsymbol{\phi}_n(s(\xi)) h_{k-1}(s(\xi)) d\xi \quad (78)$$

We can now compute the integral over the supported two-element using various numerical quadratures weights from standard tabulations such as Gauss-Legendre or Lobatto, where q is the index of the numerical quadrature point for the integral:

$$\int_{-1}^1 I_n(\mathbf{r}^0, \xi) d\xi \approx \sum_{q=1}^Q I_n(\mathbf{r}^0, \xi_q) W_q \quad (79)$$

We can follow the same procedure as above for numerically compute the outer integral of the double integral in Galerkin equation (64), also the integral for the LHS of the equation due to the local-supportedness of the basis function. For example, the integral for the LHS of Galerkin equation (64) can also be reduced into the following element integrals:

$$\begin{aligned} & \int \phi_n(\mathbf{x}) \phi_m(\mathbf{x}) dl(\mathbf{x}) \\ &= \int_{E_{k-1}} \phi_n(\mathbf{x}_{k-1}) \phi_n(\mathbf{x}_{k-1}) + \phi_n(\mathbf{x}_{k-1}) \phi_{n-1}(\mathbf{x}_{k-1}) ds \\ &+ \int_{E_k} \phi_n(\mathbf{x}_k) \phi_n(\mathbf{x}_k) + \phi_n(\mathbf{x}_k) \phi_{n+1}(\mathbf{x}_k) ds \end{aligned} \quad (80)$$

The principal cost in Galerkin methods is to evaluate the double integral in \mathbf{S}_{mn} by double-looping over elements. Matlab (matrix library) is a programming language initially developed for matrix operations. The double looping for double integrals can be effectively implemented in Matlab through multiplication between three matrixes \mathbf{ABC} . Stokeslet is first evaluated at all the quadrature points on the body, and populated into the middle matrix \mathbf{B} . The quadrature weights and basis function from each integral in the double integral of \mathbf{S}_{mn} can be populated into the two outer matrixes \mathbf{A} and \mathbf{C} , respectively.

4.5 Matrix form

The matrix form of the Galerkin equation (67) can be rewritten into a more condensed standard linear algebra form, where $\bar{\mathbf{A}}$ is a 3m-by-3n matrix populated by \mathbf{S}_{mn} , \mathbf{X} is a 3n-by-1 vector populated by \mathbf{f}_n , and \mathbf{B} is a 3m-by-1 vector populated by $\sum_{n=1}^N \mathbf{E}_{mn} \mathbf{u}_n$:

$$\bar{\mathbf{A}}\mathbf{X} = \mathbf{B}, \quad \mathbf{X} = \bar{\mathbf{A}}^{-1}\mathbf{B} \quad (81)$$

We then can use linear algebra routine to solve for \mathbf{X} given \mathbf{B} or vice versa, depending on the availability of the type of boundary conditions. If $\bar{\mathbf{A}}$ is a square matrix, it is then symmetric due to the symmetric definition of the Green's function. We can rewrite $\bar{\mathbf{A}} = \bar{\mathbf{U}}^T \bar{\mathbf{U}}$ through Cholesky decomposition [20] into the upper triangular matrix $\bar{\mathbf{U}}$, which is much more efficient to compute the inverse of a triangular matrix when multiple evaluations of the inverse of $\bar{\mathbf{A}}$ are required. We recast the linear algebra relation (81) using a more efficient form as the following in our implementations:

$$\bar{\mathbf{U}}^T \bar{\mathbf{U}} \mathbf{X} = \mathbf{B}, \quad \mathbf{X} = (\bar{\mathbf{U}}^{-1})(\bar{\mathbf{U}}^{-1})^T \mathbf{B} \quad (82)$$

Up to this point, we provided the numerical scheme for the discretized boundary integral equation in Galerkin form for a single elastic beam, in which each element of the body exerted hydrodynamic forces on itself and other elements through the relation defined by the matrix.

4.6 N-body interaction

Consider now we have a square array of total M elastic beams, and they are interacting with each other hydrodynamically. We also can discretize and solve the following new boundary integral equations using BEM, where a and b both ranging from 1 to M:

$$u_i(\mathbf{r}^b) = -\frac{1}{8\pi\mu} \sum_{a=1}^M \int S_{ij}(\mathbf{r}^b, \mathbf{r}^a) f_j(\mathbf{r}^a) dl(\mathbf{r}^a) \quad (83)$$

The hydrodynamic matrix of a single beam was formulated as $\bar{\bar{\mathbf{A}}}$ in the previous section. Since the Stokes equations are linear, we can compute the interactions between beams by assembling $\bar{\bar{\mathbf{A}}}$ as submatrixes into a larger global matrix $\bar{\bar{\mathbf{A}}}_{b,a}$. In our implementation, we first assemble the block-diagonal components of the global matrix when there are no hydrodynamic interactions between each elastic beams:

$$\bar{\bar{\mathbf{A}}}_{b,a}^D = \begin{pmatrix} \bar{\bar{\mathbf{A}}}_{1,1} & \mathbf{0} & \dots & \mathbf{0} & \mathbf{0} \\ \mathbf{0} & \bar{\bar{\mathbf{A}}}_{2,2} & \dots & \mathbf{0} & \mathbf{0} \\ \dots & \dots & \dots & \dots & \dots \\ \mathbf{0} & \mathbf{0} & \dots & \bar{\bar{\mathbf{A}}}_{M-1,M-1} & \mathbf{0} \\ \mathbf{0} & \mathbf{0} & \dots & \mathbf{0} & \bar{\bar{\mathbf{A}}}_{M,M} \end{pmatrix} \quad (84)$$

We can then populate the off-block-diagonal block by introducing the coupling submatrix $\bar{\bar{\mathbf{A}}}_{b,a}$. For example, $\bar{\bar{\mathbf{A}}}_{1,2}$ represents the hydrodynamic mobility relation exerted by beam 2 on beam 1, and $\bar{\bar{\mathbf{A}}}_{2,N}$ represents the hydrodynamic mobility relation exerted by beam N on beam 2, etc. Each row of $\bar{\bar{\mathbf{A}}}_{b,a}$ represents the hydrodynamic coupling from all other beams to the beam indexed by that row. We then have the following global hydrodynamic matrix among M beams:

$$\bar{\bar{\mathbf{A}}}_{b,a} = \begin{pmatrix} \bar{\bar{\mathbf{A}}}_{1,1} & \bar{\bar{\mathbf{A}}}_{1,2} & \dots & \bar{\bar{\mathbf{A}}}_{1,M-1} & \bar{\bar{\mathbf{A}}}_{1,M} \\ \bar{\bar{\mathbf{A}}}_{2,1} & \bar{\bar{\mathbf{A}}}_{2,2} & \dots & \bar{\bar{\mathbf{A}}}_{2,M-1} & \bar{\bar{\mathbf{A}}}_{2,M} \\ \dots & \dots & \dots & \dots & \dots \\ \bar{\bar{\mathbf{A}}}_{M-1,1} & \bar{\bar{\mathbf{A}}}_{M-1,2} & \dots & \bar{\bar{\mathbf{A}}}_{M-1,M-1} & \bar{\bar{\mathbf{A}}}_{M-1,M} \\ \bar{\bar{\mathbf{A}}}_{M,1} & \bar{\bar{\mathbf{A}}}_{M,2} & \dots & \bar{\bar{\mathbf{A}}}_{M,M-1} & \bar{\bar{\mathbf{A}}}_{M,M} \end{pmatrix}, \quad \mathbf{X}_a = \begin{pmatrix} \mathbf{X}_1 \\ \mathbf{X}_2 \\ \dots \\ \mathbf{X}_{M-1} \\ \mathbf{X}_M \end{pmatrix}, \quad (85)$$

$$\mathbf{B}_b = \begin{pmatrix} \mathbf{B}_1 \\ \mathbf{B}_2 \\ \dots \\ \mathbf{B}_{M-1} \\ \mathbf{B}_M \end{pmatrix}$$

Which also satisfy the following relations and we can solve them accordingly:

$$\mathbf{B}_b = \bar{\bar{\mathbf{A}}}_{b,a} \mathbf{X}_a \quad (86)$$

4.7 Summary of the mobility matrix

We end the chapter with a summary of the three-level of Hydrodynamic mobility matrixes that we used so far.

4.7.1 Hydrodynamic mobility matrix due to a point force: \mathbf{S} is 3-by-3

$$\mathbf{S} = \begin{pmatrix} S_{xx} & S_{xy} & S_{xz} \\ S_{yx} & S_{yy} & S_{yz} \\ S_{zx} & S_{zy} & S_{zz} \end{pmatrix} \quad (87)$$

4.7.2 Hydrodynamic mobility matrix due to a continuum body discretized by N basis function using BEM.

$$\mathbf{S}_{mn} = \begin{pmatrix} S_{x_m x_n} & S_{x_m y_n} & S_{x_m z_n} \\ S_{y_m x_n} & S_{y_m y_n} & S_{y_m z_n} \\ S_{z_m x_n} & S_{z_m y_n} & S_{z_m z_n} \end{pmatrix} \quad (88)$$

where \mathbf{S}_{mn} is 3N-by-3N, and m, n are discretization index by the basis function, which both are ranged from 1 to N.

Algorithm overview

1. compute the diagonal entry of the \mathbf{S}_{mn} with high order quadrature, where source and field element are collocated
 2. compute the off-diagonal entry of the \mathbf{S}_{mn} with low order quadrature, where source and field elements are far apart.
 3. Assemble diagonal and off-diagonal component into the matrix \mathbf{S}_{mn}
-

4.7.3 Hydrodynamic mobility matrix due to M body: $\mathbf{S}_{m,n}^{b,a}$ is 3MN-by-3MN

$$\mathbf{S}_{m,n}^{b,a} = \begin{pmatrix} \mathbf{S}_{m,n}^{1,1} & \mathbf{S}_{m,n}^{1,2} & \cdots & \mathbf{S}_{m,n}^{1,M-1} & \mathbf{S}_{m,n}^{1,M} \\ \mathbf{S}_{m,n}^{2,1} & \mathbf{S}_{m,n}^{2,2} & \cdots & \mathbf{S}_{m,n}^{2,M-1} & \mathbf{S}_{m,n}^{2,M} \\ \cdots & \cdots & \cdots & \cdots & \cdots \\ \mathbf{S}_{m,n}^{M-1,1} & \mathbf{S}_{m,n}^{M-1,2} & \cdots & \mathbf{S}_{m,n}^{M-1,M-1} & \mathbf{S}_{m,n}^{M-1,M} \\ \mathbf{S}_{m,n}^{M,1} & \mathbf{S}_{m,n}^{M,2} & \cdots & \mathbf{S}_{m,n}^{M,M-1} & \mathbf{S}_{m,n}^{M,M} \end{pmatrix} \quad (89)$$

where m, n are discretization index by the basis function which both are ranged from 1 to N.

Algorithm overview

1. Repeat the process for single beam calculations for N beams, and assemble them to the block diagonal of the global matrix using “parfor” (Matlab), $\mathbf{S}_{m,n}^{b,a}$
 2. Compute the off-block diagonal submatrix only in the upper triangular part of the global matrix, $\mathbf{S}_{m,n}^{b,a}$
 3. Taking the transpose of the upper triangular matrix to get the lower triangular part of the matrix due to the symmetric properties from Galerkin method
-

Chapter 5 Results and Discussions

In this chapter, we apply the mathematical model presented in previous chapters to two physical setups to demonstrate the capability of the proposed numerical method for solving the flow field created by the evolving boundaries of the microcantilevers. In section 5.1, we inspect the behaviors of the array under an externally imposed shear flows. In section 5.2, we exam the flow field generated by an actively driven array in stagnant fluids. Finally, in section 5.3, we discuss the effect of the wall presence on the cantilever arrays, which exhibit very different flow fields than when they are far from the wall leading to implication on the formation of the distinct mixing region along the length of cantilevers. Our numerical methods achieved fourth-order spatial accuracy for passive array undergoes external flow and second-order accuracy for actively-driven array in stagnant fluids.

5.1 Passive cantilevers under a Couette Flow

A straight 9-by-9 cantilevers array is placed vertically in the \mathbf{x} - \mathbf{z} plane with an externally imposed unidirectional Couette flow, $u(z)$, in the \mathbf{x} -direction, and the array is fixed to a rigid wall at the bottom, and its top-end is stress-free and free to move in the fluids. h is the height of the channel, and U_0 is the maximum velocity of the external flow.

$$u(z) = U_0 \frac{z}{h} \tag{90}$$

The spatially discretized EOM of the elastic beam is parametrized by two effective drag coefficients. C_1 relates to the strength of hydrodynamic coupling between each beam, and C_2 to the effect of the externally imposed flow on all beams.

$$\frac{d^2 \mathbf{x}_n}{dt^2} = (\mathbf{A} \mathbf{x}_n + \mathbf{b}_n) - C_1 \mathbf{R} \mathbf{u}_n + C_2 \mathbf{R} \mathbf{u}_n^\infty, \quad C_1 = \sqrt{\frac{\mu^2 L^4}{\rho EI}}, C_2 = \frac{\mu L^4 \lambda}{EI} \quad (91)$$

In our simulation examples, the cantilevers are made of silicon nitride, which has a length of 1mm and radius of 1um, Young E modulus of 160 GPa, and a density of 15kg/m. We set the external Couette flow velocity $U_0 = 1 \text{ mm/s}$, $\mu = 3cP$, and $Re = 0.3$. When we simulated the array with very stiff materials such as silicon nitride, the array reaches steady-state quickly with a minimal deflection from its equilibrium position and behave almost like a rigid body to divert the flow field. Since the Stokes flow is linear, we can decompose it into an externally applied flow and disturbance flow. The disturbance field is a result of fluid-structure interaction of the array when they respond to the external flow fields to satisfy no-slip boundary condition on the beams. The superposition of the external and disturbance field is the actual flow field in the fluid.

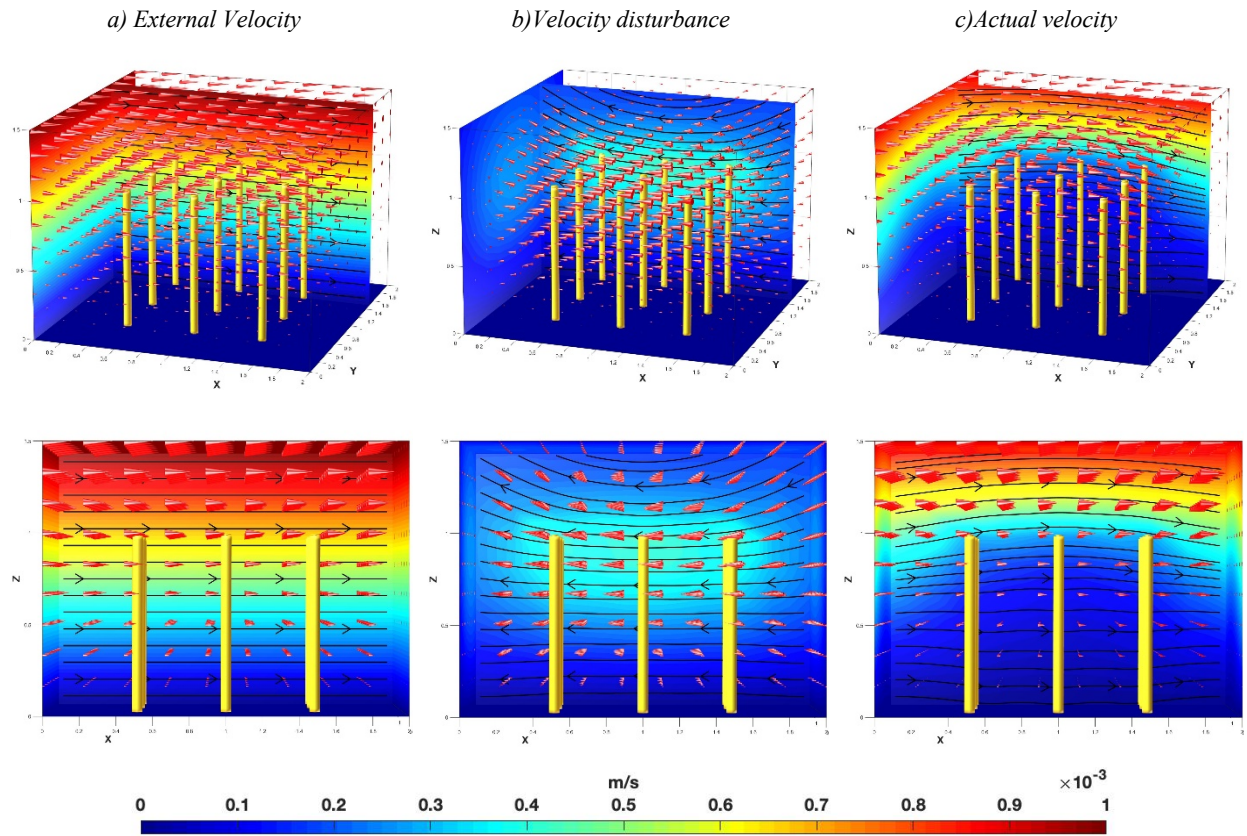


Figure 3 The first row is the 3D view, and the second row is the side view of the cantilever array. The color map is the velocity magnitude of the flow in m/s. a) external Couette flow with $U_0 = 1 \text{ mm/s}$; b) the fluid disturbance generated by the array; c) superposition of a and b equal to the actual flow field

Under the same setup in figure 3 with silicon nitride, we immersed the array in fluids with different viscosities ranging from 3×10^{-4} to $3 \times 10^{-3} Pa \cdot s$ corresponding to the physiological fluids at $37 C^0$. The effective drag coefficient exerted by the external flow, $C_2 = \frac{\mu L^4 \lambda}{EI}$, is linearly proportional to the viscosity, μ . When the viscosity increase, the beam tip has a larger deflection from its natural position since the external flow exerted a more significant drag on them. When the viscosity decrease, the tip has a smaller deflection since a smaller drag is experienced by the beam. Figure 4 a) demonstrated the evolution of one beam tip immersed in fluids with different viscosity. Figure 4b) shows the relationship between the steady-state beam tip deflections against different viscosity values.

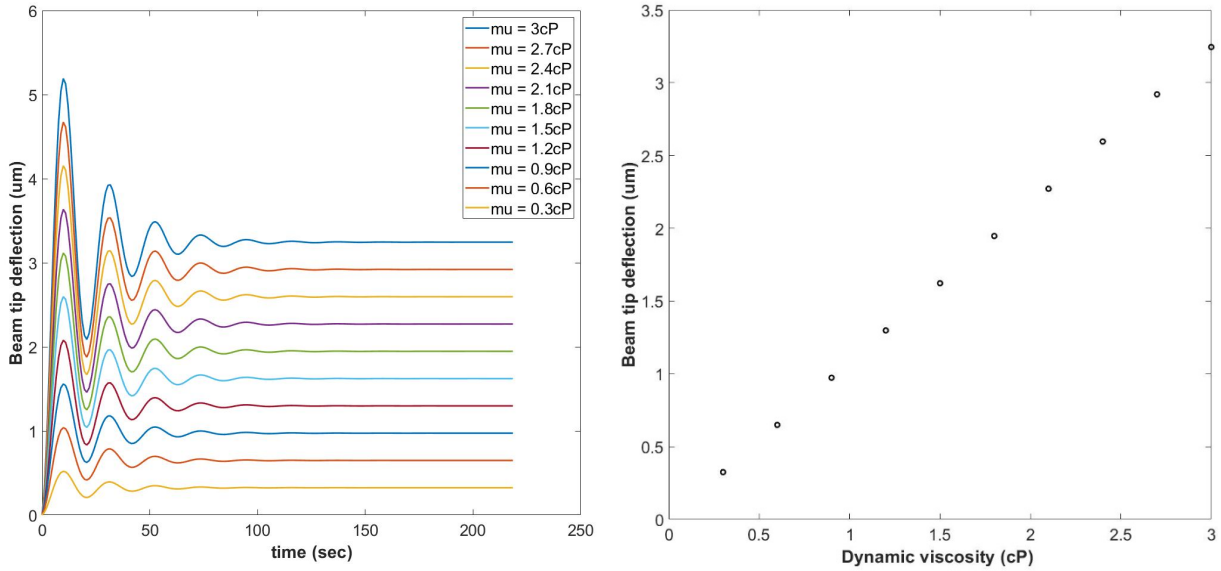


Figure 4 Cantilever immersed in fluids with different viscosities. a) Time evolution of a single beam tip deflections. b) The steady-state beam deflection immersed in fluids with different viscosities

When we reduce the stiffness, E , of the cantilever beams by 2 order of magnitude to 1.6 GPa, we obtain bent beams array with visible oscillation in x directions before reaching steady states, and also we observed small emergent oscillatory motion in the x-y plane of the array due to the hydrodynamic interactions. The following figure shows the simulation snapshot at the

steady-state, where the final flow field adjusted accordingly to the evolving cantilevers boundary by shifting the flow field symmetry to the right.

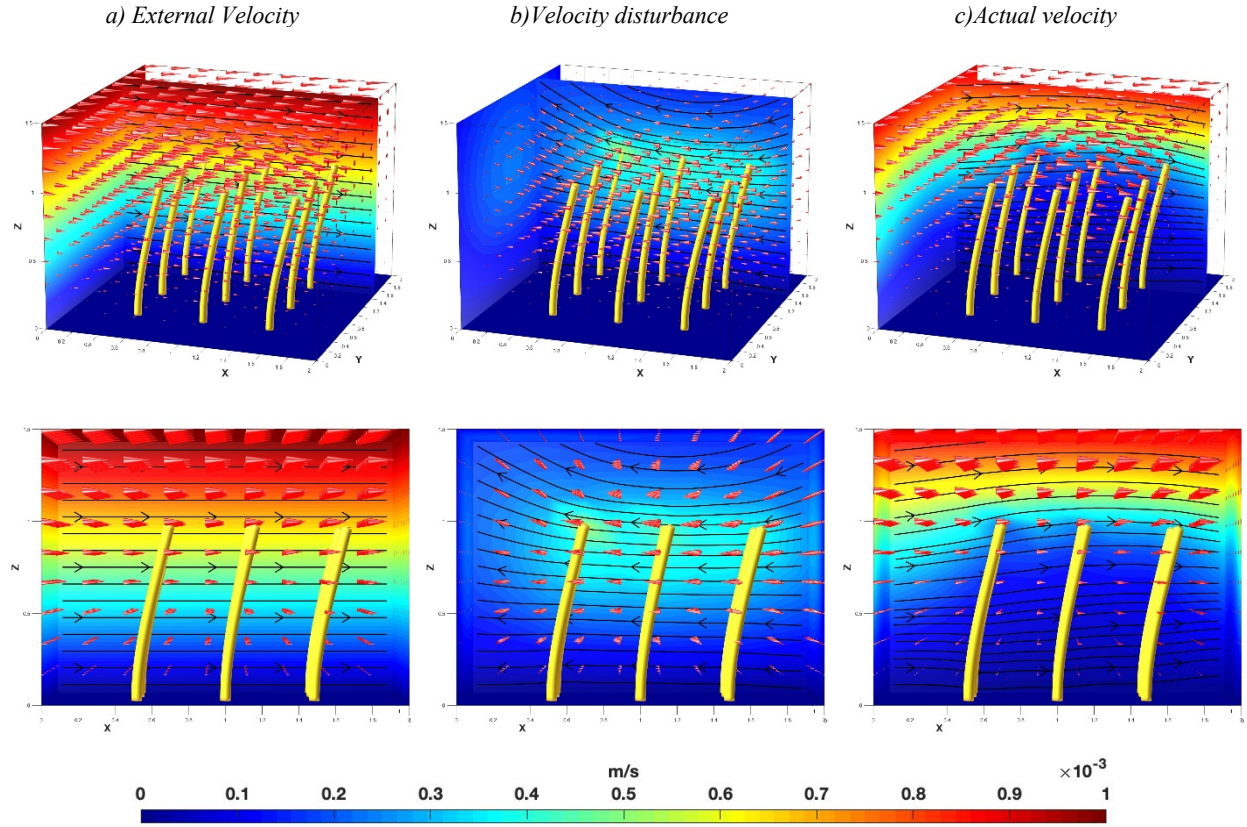


Figure 5 The first row is the 3D view, and the second row is the side view of the cantilever array. The color map is the velocity magnitude of the flow in m/s. a) external Couette flow with $U_0 = 1\text{mm/s}$; b) the fluid disturbance generated by the array; c) superposition of a and b equal to the actual flow field

5.1.1 Convergence and accuracy

To evaluate the order of accuracy of the proposed numerical method, we compute the same runs of simulations with refining parameters of spatial resolutions of the elastic beams with $N = 10, 20,$ and 40 .

$$\log_2 \left(\frac{\tilde{X}_h - \tilde{X}_{h/2}}{\tilde{X}_{h/2} - \tilde{X}_{h/4}} \right) = p + O(h) \quad (92)$$

We compare solutions when ‘h’ is halved successively, where h is the spatial discretization resolution, and \tilde{X}_h is the tip of each elastic beams in the array. From figure 6a), we can see that when we increased the number of discretization points for the cantilevers, the solution of the cantilever tip converged. The figure 6b) shows the order of accuracy of the cantilever beams with setup in figure 1 calculated from (92), with an average of fourth-order accuracy over time.

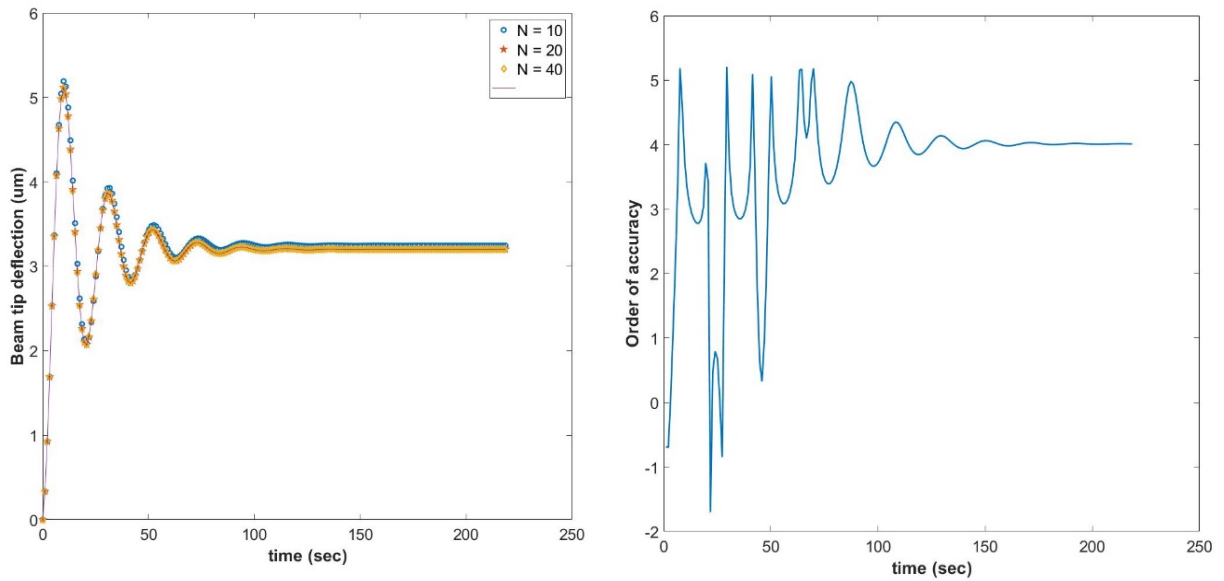


Figure 6 Comparison between solutions from run with cantilevers with the same physical setups but the different number of spatial discretization points $N = 10$, $N = 20$ and $N = 40$. a) Tip displacement in x-direction over time for one of the cantilevers beam in the array. B) The order of accuracy approximation calculated for the cantilever array using formula (92).

5.2 Actively-driven cantilever array in stagnant fluids

In this section, we will exam the behavior of an actively-driven microcantilevers array inside a stagnant fluid with one end of the cantilevers fixed to the wall and the other stress-free

and free to move. In the absence of external flow, we have the following equation characterized by a single dimensionless parameter C_1 :

$$\frac{d^2 \mathbf{x}_n}{dt^2} = (\mathbf{A}\mathbf{x}_n + \mathbf{b}_n + \mathbf{F}_{drive}) - C_1 \mathbf{R}\mathbf{u}_n, \quad C_1 = \sqrt{\frac{\mu^2 L^4}{\rho EI}} \quad (93)$$

In this simulation, we keep all the parameters as previous sections but only introduced an external driving force, \mathbf{F}_{drive} . It is a square wave toggle between positive and negative \mathbf{x} -direction in time with the magnitude on the order of characteristic elastic force $\mathbf{F}_{drive} \sim \frac{EI}{L^3}$. The results in figure 7 show a three-dimensional flow field of one complete driving cycle of the array. An increase in horizontal transport due to the array motion is found where the fluids are being drawn in from one side and push out to the other. Also, we notice the rapid decay of the flow field in the vertical directions due to the presence of the wall forming a stagnant layer region surrounding the lower bottom half of the cantilevers. The mass transport process in these is dominated by molecular diffusion rather than convective transport compared to the top half region.

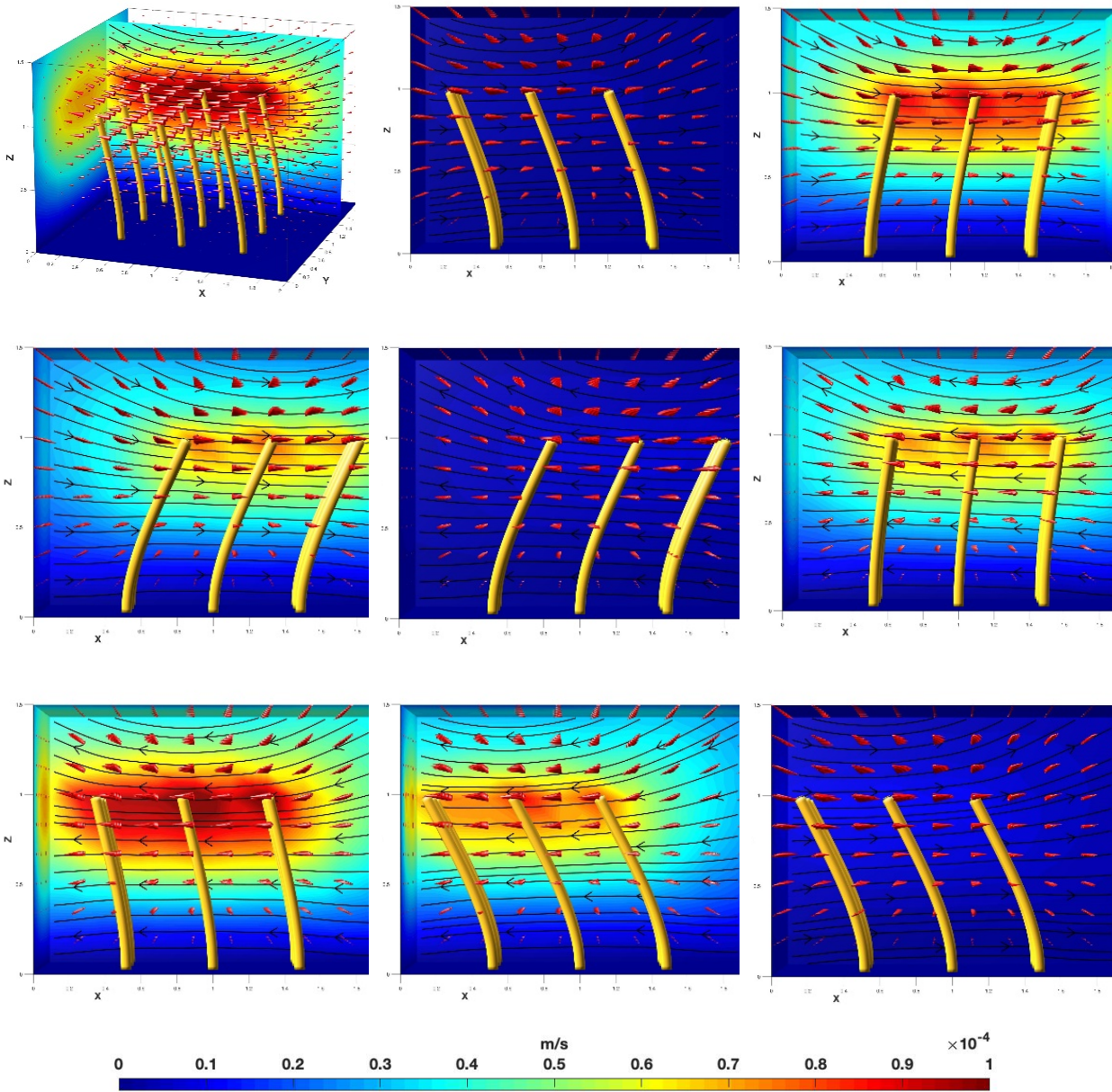


Figure 7 the complete one cycles of the beat pattern of the array driven by a square wave with a period of 21 seconds

5.2.1 Convergence and accuracy

Figures 8 and 9 below show the spatial convergence and the order of accuracy of the numerical method when the array is driven by an external square wave with different periods.

For example, we obtain a time-averaged order of accuracy of 2.1851 with a period of 21 seconds, and 2.1579 with a period of 1 min.

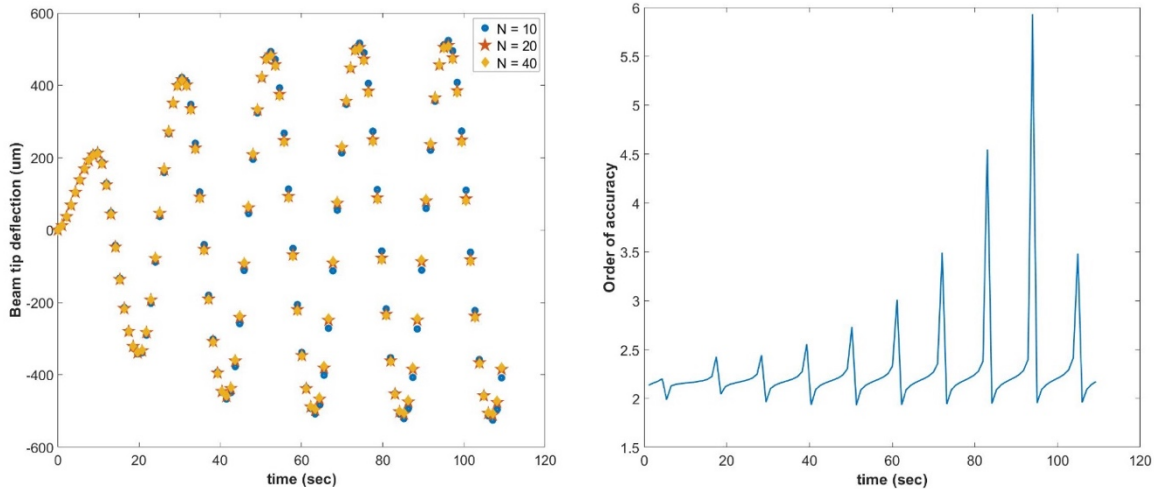


Figure 8 Cantilever array driven by a square wave with 21 second period. Comparison between solutions from run with cantilevers with a different number of spatial discretization points $N = 10$, $N = 20$ and $N = 40$. a) Tip displacement in x-direction over time for one of the cantilevers beam in the array. B) The order of accuracy approximation calculated for the entire array using formula (92).

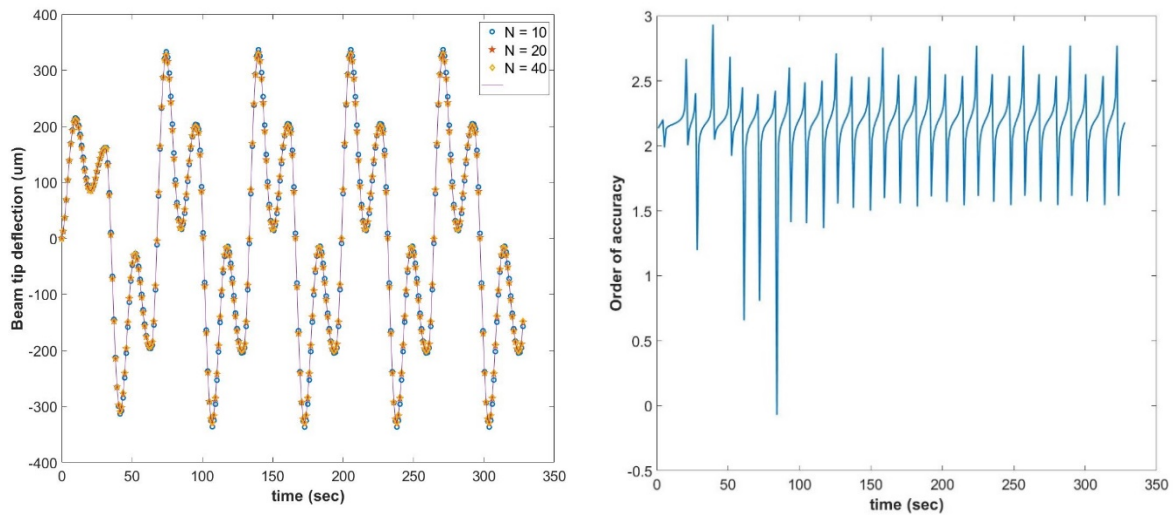


Figure 9: Cantilever array driven by a square wave with 1 min period

5.3 The effect of the wall

In the final example, we compare the simulation of flow fields with and without the presence of the wall, and we also increase the size of the cantilever array into 100. Figure 10 shows a simulation snapshot of the array with different viewing angles at the same instance of time. The

first-row simulation included the effect of the wall and the second row without. In the presence of the wall, a distinct stagnant fluid region can be found surrounding the lower half regions of the beams in contrast to the intense mixing effect at the upper half region. The wall effectively acts as a momentum sink to dissipate the kinetic energy of the flow to satisfy no-slip boundary conditions. In the absence of the wall, a higher overall velocity can be observed, and the fluids can pass freely through the bottom leading to a strong vertically suction and pumping effect, and the mixing effect along the beams is nearly homogenous in contrast to the formation of the distinct mixing region for the array bounded by the wall.

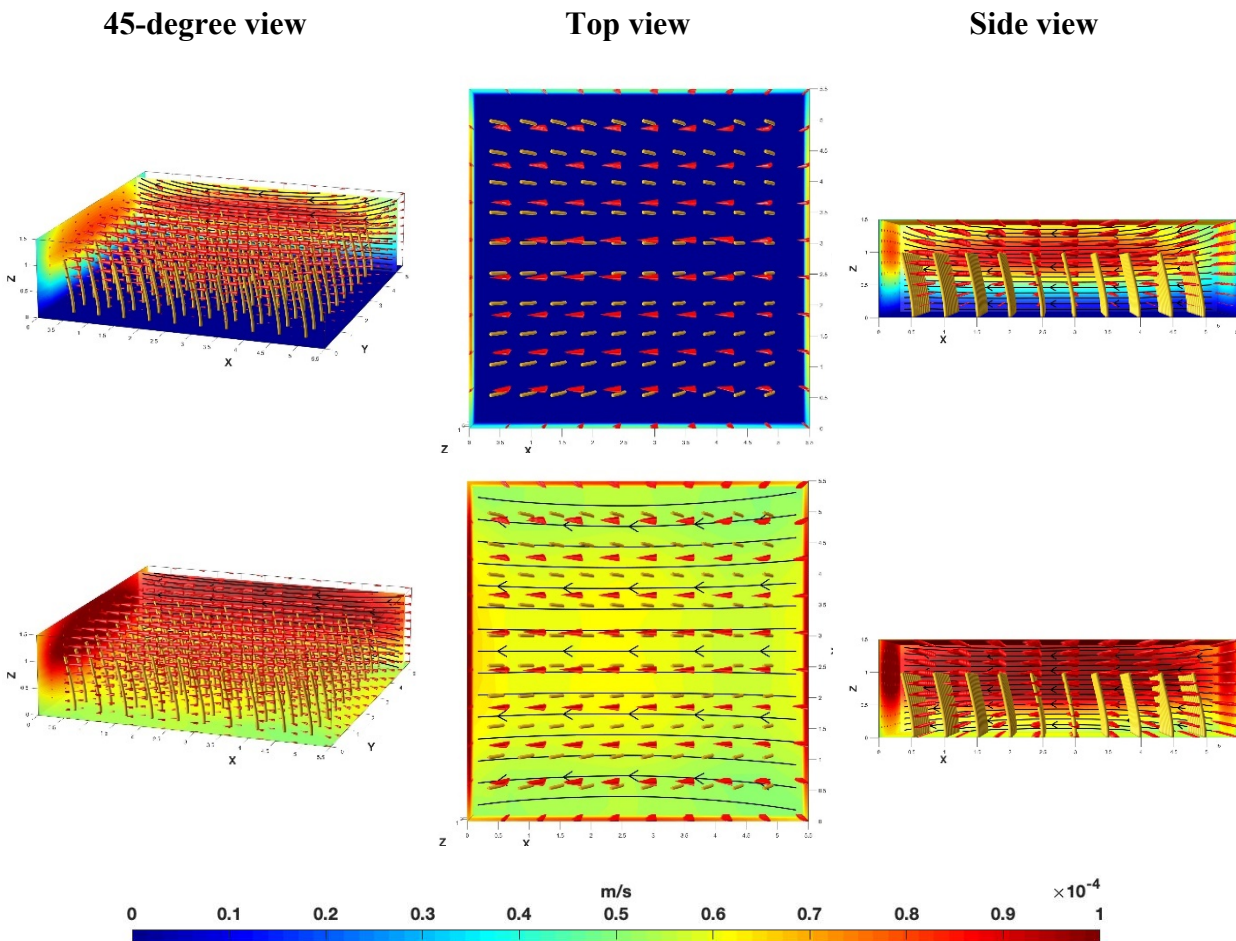


Figure 10, the first row: the flow field generated by the array bounded by the wall; the second row: the flow field generated by the array anchored far from the wall. The color map represents the magnitude of the velocity. The snapshots are taken at the same instance of time

The final figure demonstrates simulation snapshots of the 100-cantilever array bounded by a wall undergoes one cycle. The simulation was done on a standard desktop computer.

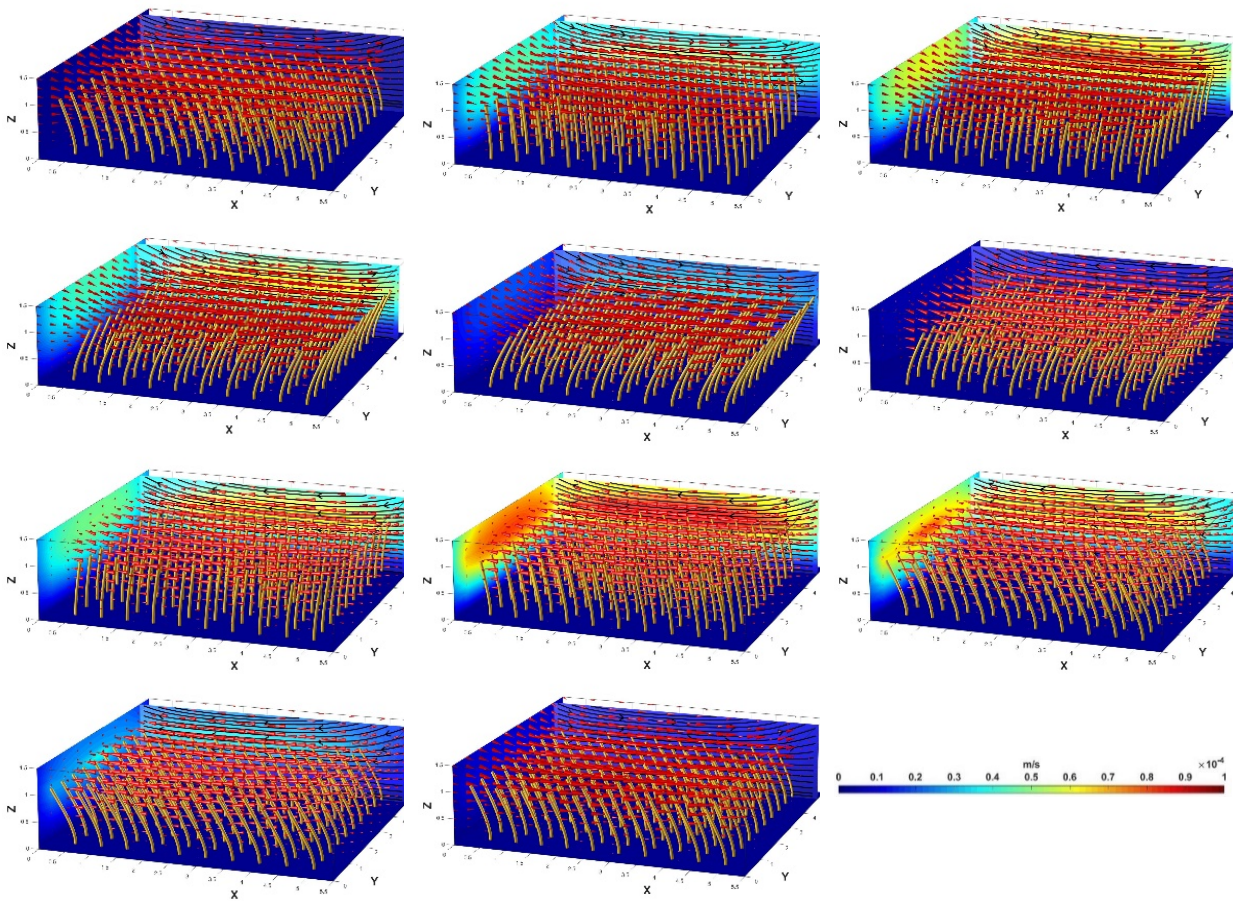


Figure 11 One complete beat pattern of 100 actively-driven microcantilevers bounded by a wall. Colormap represents velocity magnitude

Chapter 6 Conclusions

In this thesis, we presented the boundary integral formulation of multiple elastic beams immersed in Stokes flow bounded by a wall, and its numerical solution by the boundary element method. The accuracy and convergence properties of the method were examined in chapter 5 along with two different example applications of the array passively reacting to external shear flow and the array actively-driving in stagnant fluids. Our numerical methods demonstrated 4th order spatial accuracy for the passive array and 2nd order accuracy for the active array. We also investigated the effect of a range of viscosity on the passive arrays that undergo external shear flow and the effect of the wall in the actively-driven array. Finally, we demonstrate the capability of the current numerical methods for resolving a large number of elastic beams interactions up to 100 on a desktop computer, which would require supercomputer resources if standard commercial software was used. The motivation of using the Boundary integral formulation to model zero Reynolds applications is because the volumetric discretization of the fluid domain is avoided by taking advantage of the known Green's function. The motivation of using the Boundary element method for discretizing the integral equation compared to the standard Nystrom method is to decouple the dependency between force and quadrature discretization. The method can be easily adapted for various applications. The test cases of the array with external flow and force in this thesis are examples of such. Through several numerical examples and applications, this method has been derived, implemented, and verified. However, many biological applications are interesting to be investigated and explored, which required further validation and experimental data, for example, using the atomic force microscope. The focus of the thesis is to build up a numerical platform which would enable future studies in interesting applications combined with experimental studies.

Appendixes

A. Equation of motion without beam inertia

The inertia does not affect the constitutive relations here. If the beams have negligible inertias, we can have the forces-free EOM:

$$0 = \mathbf{F}^{elastic}(\mathbf{X}) + \mathbf{F}^{hydro}(\mathbf{U}) \quad (94)$$

$$0 = (-EI\mathbf{X}_{ssss} + b\mathbf{X}_{ss}) - \mu\mathcal{L}(\mathbf{U} - \mathbf{u}_{bg}) \quad (95)$$

The equation can be scaled as follows:

$$0 = \frac{EI}{L^3}(-\mathbf{X}^*_{ssss} + \mathbf{X}^*_{ss}) - \frac{\mu L}{T_1}\mathcal{L}\mathbf{U}^* + \frac{\mu L}{T_2}\mathcal{L}\mathbf{u}_{bg}^* \quad (96)$$

We can rearrange the above equation to obtain:

$$\frac{\mu L}{T_1}\mathcal{L}\mathbf{U}^* = \frac{EI}{L^3}(-\mathbf{X}^*_{ssss} + \mathbf{X}^*_{ss}) + \frac{\mu L}{T_2}\mathcal{L}\mathbf{u}_{bg}^* \quad (97)$$

Divide both sides by $\frac{\mu L}{T_1}$ and multiply both sides with \mathcal{L}^{-1} , we obtain the dimensionless equation:

$$\mathbf{U}^* = \frac{T_1 EI}{\mu L^4}\mathcal{L}^{-1}(-\mathbf{X}^*_{ssss} + \mathbf{X}^*_{ss}) + \frac{T_1}{T_2}\mathbf{u}_{bg}^* \quad (98)$$

Assume that the drag forces due to the beam motions (\mathbf{U}) and the internal elastic forces are on the same order of magnitude, we can set the time scale T_1 to the relaxation time of the elastic beams, and keep T_2 as the characteristic time scale of the imposed flow.

$$T_1 = \frac{\mu L^4}{EI}, \quad T_2 = \frac{1}{\lambda} \quad (99)$$

We obtain the final dimensionless equation with no inertia beam characterized by a single parameter C_1 :

$$\mathbf{U} = \mathcal{L}^{-1}(-\mathbf{X}^*_{ssss^*} + \mathbf{X}^*_{ss^*}) + C_1 \mathbf{u}_{bg}$$

$$C_1 = \frac{\mu L^4 \lambda}{EI} \quad (100)$$

We can have the following spatially discretized equation of motions:

$$0 = \mathbf{R}\mathbf{u}_n + \mathbf{A}\mathbf{x}_n + \mathbf{b}_n \quad (101)$$

$$\mathbf{u}_n = -\mathbf{R}^{-1}(\mathbf{A}\mathbf{x}_n + \mathbf{b}_n) \quad (102)$$

We can also discretize this in time as:

$$\mathbf{x}_n^{t+1} = \mathbf{x}_n^t - \mathbf{R}^{(t)-1}(\mathbf{A}\mathbf{x}_n^{t+1} + \mathbf{b}_n)dt \quad (103)$$

And solve the solid mechanics implicitly in time, and fluid explicitly:

$$\mathbf{x}_n^{t+1} = \left(I + \mathbf{R}^{(t)-1} \mathbf{A} dt \right)^{-1} \left(\mathbf{x}_n^t - \mathbf{R}^{(t)-1} \mathbf{b}_n dt \right) \quad (104)$$

B. Fundamental solutions of Stokes equation in free space

In this section, we derive the Green's function of Stokes flow in free space. Considering a particular flow configuration at x_i as a result of a point force f_i applied at x_i^0 to Stokesian fluids, the singularly forced momentum equation reads:

$$0 = -\frac{\partial P}{\partial x_i} + \mu \frac{\partial^2 u_i}{\partial x_j^2} + f_i \delta(r) = \frac{\partial \sigma_{ij}}{\partial x_j} + f_i \delta(r) \quad (105)$$

where $\hat{x}_i = x_i - x_i^0$, $r = \sqrt{\hat{x}_i \hat{x}_i}$, and $\delta(r)$ is a three-dimensional Dirac function such that

$$\begin{cases} \delta(r) = 0, & \text{for } x_i \neq x_i^0 \\ \delta(r) = \infty, & \text{for } x_i = x_i^0 \end{cases} \quad (106)$$

$$\iiint \delta(x_i - x_i^0) f_i dV(x_i) = f_i \quad (107)$$

where the volume integral took place on arbitrary domain enclosed x_i^0 . Laplace's equation has a well-known fundamental solution of the following:

$$\frac{\partial^2 G(r)}{\partial x_i^2} = \delta(r), \quad G(r) = -\frac{1}{4\pi r} \quad (108)$$

We can substitute the expression for Dirac delta into the Stokes momentum equation, and get:

$$0 = -\frac{\partial P}{\partial x_i} + \mu \frac{\partial^2 u_i}{\partial x_j^2} + f_i \frac{\partial^2 G}{\partial x_i^2} \quad (109)$$

Taking the divergence of the above equation and apply the continuity equation, we get:

$$\frac{\partial^2 P}{\partial x_i^2} = \frac{\partial^2}{\partial x_i^2} \left(f_i \frac{\partial G}{\partial x_i} \right) \quad (110)$$

The pressure is then:

$$P = f_i \frac{\partial G}{\partial x_i} \quad (111)$$

Substitute the pressure back to the Stokes's momentum, and we obtain the following:

$$\frac{\partial^2 u_i}{\partial x_j^2} = \frac{f_j}{\mu} \left(\frac{\partial^2}{\partial x_i \partial x_j} - \delta_{ij} \frac{\partial^2}{\partial x_i^2} \right) G \quad (112)$$

Let's simplify the expression the above equation a little by defining a new linear differential operator, $\tilde{\mathcal{L}}$:

$$\tilde{\mathcal{L}} := \frac{f_j}{\mu} \left(\frac{\partial^2}{\partial x_i \partial x_j} - \delta_{ij} \frac{\partial^2}{\partial x_i^2} \right) \quad (113)$$

The singularly forced Stokes momentum equation:

$$\frac{\partial^2 u_i}{\partial x_j^2} = \tilde{\mathcal{L}} G \quad (114)$$

We can presume a velocity ansatz of similar form that match the RHS:

$$u_i = \tilde{\mathcal{L}} H \quad (115)$$

Substitute velocity ansatz into Stokes momentum and interchange the order of the differentiation, rearrange equations, and we get:

$$\tilde{\mathcal{L}} \left(\frac{\partial^2 H}{\partial x_j^2} - G \right) = 0 \quad (116)$$

To satisfy the above equation, we can solve for the Poisson equation:

$$\frac{\partial^2 H}{\partial x_j^2} = G \quad (117)$$

Taking Laplacian of the above equation, we get a singularly forced Biharmonics equation:

$$\begin{aligned} \frac{\partial^2}{\partial x_j^2} \frac{\partial^2 H}{\partial x_j^2} &= \frac{\partial^2 G}{\partial x_j^2} \\ \frac{\partial^4 H(r)}{\partial x_j^4} &= \delta(r) \end{aligned} \quad (118)$$

The biharmonic equation has a well-known Green's function as:

$$H(r) = -\frac{r}{8\pi} \quad (119)$$

Substitute biharmonic Green's function back to into velocity ansatz, and we then obtain the Green's function for the velocity field, S_{ij} , for the Stokes equation:

$$\begin{aligned} u_i &= \frac{f_j}{\mu} \left(\frac{\partial^2 H}{\partial x_i \partial x_j} - \delta_{ij} \frac{\partial^2 H}{\partial x_i^2} \right) = \frac{f_j}{8\pi\mu} \left(\delta_{ij} \frac{\partial^2 r}{\partial x_i^2} - \frac{\partial^2 r}{\partial x_i \partial x_j} \right) \\ &= \frac{f_j}{8\pi\mu} \left(\frac{\hat{x}_j \hat{x}_i}{r^3} + \frac{1}{r} \delta_{ij} \right) = \frac{f_j}{8\pi\mu} S_{ij} \end{aligned} \quad (120)$$

Upon checking, Stokeslet satisfies the continuity equation by their construction:

$$\frac{\partial S_{ij}}{\partial x_i} = \frac{-\delta_{ij} \hat{x}_i}{r^3} + \frac{\delta_{ii} \hat{x}_j + \delta_{ij} \hat{x}_i}{r^3} - \frac{3\hat{x}_i \hat{x}_j \hat{x}_k}{r^5} = 0 \quad (121)$$

The free space pressure green's function is proportional to Laplacian dipole:

$$P = f_i \frac{\partial G}{\partial x_i} = \frac{f_i}{8\pi} \frac{2x_i}{r^3} = \frac{f_i}{8\pi} P_i \quad (122)$$

$$P_i = \frac{2x_i}{r^3} \quad (123)$$

Substituting velocity and pressure in terms of their respective Green's function into the incompressible Newtonian constitutive relation, we established the relation between stress tensor's green function to velocity and pressure green's functions:

$$T_{ijk} = -\delta_{ik} \frac{2x_j}{r^3} + \frac{\partial S_{ij}}{\partial x_k} + \frac{\partial S_{kj}}{\partial x_i} \quad (124)$$

$$T_{ijk} = -6 \frac{x_j x_k x_i}{r^5} \quad (125)$$

C. source dipole, force dipole, and multipole

In this section, we will briefly introduce the idea of dipoles and higher-order multipoles generalization in the singularity methods. We first show how the mass conservation equations respond to an applied singular point source. Its physical analogy would be injecting fluids with a needle into a large domain [14], whereas Stokeslet represents the response from hitting the fluids with a hammer at a point. The singularly forced continuity equation reads:

$$\frac{\partial u_i}{\partial x_i} = q\delta(r) \quad (126)$$

The potential flow solution satisfies the mass conservation equation above:

$$u_i = \frac{\partial \phi}{\partial x_i} \quad (127)$$

Substitute (127) into (126), we have the Laplace equation:

$$\frac{\partial^2 \phi}{\partial x_i^2} = q\delta(r) \quad (128)$$

ϕ is proportional to the Laplacian's green's function:

$$\phi = qG(r) \quad (129)$$

The velocity due to point source injection, q , is, therefore:

$$u_i = \frac{\partial \phi}{\partial x_i} = q \frac{\partial G(r)}{\partial x_i} = \frac{1}{4\pi} \frac{\hat{x}_i}{r^3} = \frac{1}{4\pi} M_i q \quad (130)$$

M_i is the Green's function due to a point source:

$$M_i = \frac{\hat{x}_i}{r^3} \quad (131)$$

Let us now consider that the point source injection point is at x_i' which is at some small distance away from x_i^0 . We can represent response at a distance away in terms of injection at x_i^0 by using Taylor series expansions of the Green's function.

$$\begin{aligned}
M_i(x_i, x_i') &= M_i(x_i, x_i^0) + (x_j^0 - x_j') \frac{\partial M_i(x_i, x_i^0)}{\partial x_j} \\
&+ \frac{1}{2} (x_k^0 - x_k') (x_j^0 - x_j') \frac{\partial^2 M_i(x_i, x_i^0)}{\partial x_k \partial x_j} + H. O. T.
\end{aligned} \tag{132}$$

The first term contributes to point source monopole, second term to dipole and third term quadrupole, etc. The dipole and higher-order poles can be easily found through some simple differentiation operations:

$$\frac{\partial M_i}{\partial x_j} = \frac{\partial}{\partial x_j} \left(\frac{\hat{x}_i}{r^3} \right) = \frac{1}{r^3} \frac{\partial \hat{x}_i}{\partial x_j} - \frac{3\hat{x}_i}{r^4} \frac{\partial r}{\partial x_j} = \frac{\delta_{ij}}{r^3} - \frac{3\hat{x}_i \hat{x}_j}{r^5} \tag{133}$$

$$\frac{\partial M_i}{\partial x_k \partial x_j} = \frac{\partial}{\partial x_k \partial x_j} \left(\frac{\hat{x}_i}{r^3} \right) = 15 \left(\frac{\hat{x}_i \hat{x}_j \hat{x}_k}{r^7} - \frac{\hat{x}_i \delta_{jk} + \hat{x}_j \delta_{ki} + \hat{x}_k \delta_{ij}}{5r^5} \right) \tag{134}$$

The same idea of Taylor series expansions can also be applied to the Stokeslet. We can approximate the fluid velocity response, $S_{ij}(x_i, x_i')$, at x_i' due to a point force applied some distance way at x_i^0 by using Taylor series expansions as following:

$$\begin{aligned}
S_{ij}(x_i, x_i') &\approx S_{ij}(x_i, x_i^0) + (x_k^0 - x_k') \frac{\partial S_{ij}(x_i, x_i^0)}{\partial x_k} \\
&+ \frac{1}{2} (x_m^0 - x_m') (x_k^0 - x_k') \frac{\partial^2 S_{ij}(x_i, x_i^0)}{\partial x_m \partial x_k} + H. O. T.
\end{aligned} \tag{135}$$

The Stokeslet dipole can be easily found as the following:

$$\frac{\partial S_{ik}}{\partial x_j} = -\frac{1}{8\pi\mu} \left(\frac{x_j \delta_{ik} - x_k \delta_{ij} - x_i \delta_{kj}}{r^3} + 3 \frac{x_j x_i x_k}{r^5} \right) \tag{136}$$

D. Boundary integral equations

Reciprocal relations

The reciprocal theorem [10] is the most useful tool for the study of stokes flow, and it provides the theoretical foundation for formulating the boundary integral equations. It gives a relationship between two different Stokes flows under the same domain. Typically, one flow has the known fundamental solutions, and the other is an unknown complex flow as the solution to a particular problem. Consider two independent Stokesian flows u_j^a and u_j^b with respective stress tensors σ_{ij}^a and σ_{ij}^b , we compute the projection of Stokes equations of flow “a” onto the velocity of flow “b” and substitute the constitutive relation of the Newtonian stress tensor σ_{ij} :

$$\begin{aligned}
 u_j^b \frac{\partial \sigma_{ij}^a}{\partial x_i} &= \frac{\partial u_j^b \sigma_{ij}^a}{\partial x_i} - \sigma_{ij}^a \frac{\partial u_j^b}{\partial x_i} \\
 &= \frac{\partial u_j^b \sigma_{ij}^a}{\partial x_i} - \left(-p^a \delta_{ij} + \mu \left(\frac{\partial u_i^a}{\partial x_j} + \frac{\partial u_j^a}{\partial x_i} \right) \right) \frac{\partial u_j^b}{\partial x_i} \\
 &= \frac{\partial u_j^b \sigma_{ij}^a}{\partial x_i} + p^a \frac{\partial u_i^b}{\partial x_i} - \mu \left(\frac{\partial u_i^a}{\partial x_j} + \frac{\partial u_j^a}{\partial x_i} \right) \frac{\partial u_j^b}{\partial x_i}
 \end{aligned} \tag{137}$$

Applied the continuity constraints, $\frac{\partial u_i^b}{\partial x_i} = 0$, we obtain the Green’s first identity for

Stokes equations:

$$u_j^b \frac{\partial \sigma_{ij}^a}{\partial x_i} = \frac{\partial u_j^b \sigma_{ij}^a}{\partial x_i} - \mu \left(\frac{\partial u_i^a}{\partial x_j} + \frac{\partial u_j^a}{\partial x_i} \right) \frac{\partial u_j^b}{\partial x_i} \tag{138}$$

Switching the order of the flow, we can obtain a second relation:

$$u_j^a \frac{\partial \sigma_{ij}^b}{\partial x_i} = \frac{\partial u_j^a \sigma_{ij}^b}{\partial x_i} - \mu \left(\frac{\partial u_i^b}{\partial x_j} + \frac{\partial u_j^b}{\partial x_i} \right) \frac{\partial u_j^a}{\partial x_i} \tag{139}$$

The generalized reciprocal relations for stokes flow can be obtained through subtracting equation (139) from (138) as the following:

$$u_j^b \frac{\partial \sigma_{ij}^a}{\partial x_i} - u_j^a \frac{\partial \sigma_{ij}^b}{\partial x_i} = \frac{\partial u_j^b \sigma_{ij}^a - u_j^a \sigma_{ij}^b}{\partial x_i} \quad (140)$$

If two flows both satisfy the Stokes equation in the absence of external forces, the LHS of the equations would be zeros as $\frac{\partial \sigma_{ij}^a}{\partial x_i} = \frac{\partial \sigma_{ij}^b}{\partial x_i} = 0$ for stokes momentum, yielding the special reciprocal relation (Lorentz's relations):

$$\frac{\partial}{\partial x_i} (u_j^b \sigma_{ij}^a - u_j^a \sigma_{ij}^b) = 0 \quad (141)$$

Boundary integral equations

Considering we have two independent Stokes flow on the same domain where flow “a” does not have any external force, while flow “b” has an external point force as $\delta(x_i, x_i^0) f_j$.

Stokes flow a:

$$\frac{\partial \sigma_{ij}^a}{\partial x_i} = 0 \quad (142)$$

Stokes flow b:

$$\frac{\partial \sigma_{ij}^b}{\partial x_i} = -\delta(x_i, x_i^0) f_j \quad (143)$$

We then substitute two flows into the generalized reciprocal relations (140) together with Stokes flow Green's functions to obtain the following relations:

$$\delta(\mathbf{x}, \mathbf{x}^0) u_k^a = \frac{\partial}{\partial x_i} \left(\frac{1}{8\pi\mu} S_{jk}(\mathbf{x}, \mathbf{x}^0) \sigma_{ij}^a - u_j^a \frac{1}{8\pi} T_{ikj}(\mathbf{x}, \mathbf{x}^0) \right) \quad (144)$$

Integrate the differential equations above over a close control volume:

$$\iiint \delta(\mathbf{x}, \mathbf{x}^0) u_k^a dV = \iiint \frac{\partial}{\partial x_i} \left(\frac{1}{8\pi\mu} S_{jk}(\mathbf{x}, \mathbf{x}^0) \sigma_{ij}^a - u_j^a \frac{1}{8\pi} T_{ikj}(\mathbf{x}, \mathbf{x}^0) \right) dV \quad (145)$$

Applied divergence theorem to convert the RHS volume integral into a surface integral, and the LHS integral vanishes to a point due to the property of 3D Dirac delta function, and we then obtain the boundary integral equation for Stokes flow:

$$\begin{aligned}
u_k(\mathbf{x}^0) = & -\frac{1}{8\pi\mu} \iint S_{jk}(\mathbf{x}, \mathbf{x}^0) \sigma_{ij}(\mathbf{x}) n_i(\mathbf{x}) dS(\mathbf{x}) \\
& + \frac{1}{8\pi} \iint u_j(\mathbf{x}) T_{ikj}(\mathbf{x}, \mathbf{x}^0) n_i(\mathbf{x}) dS(\mathbf{x})
\end{aligned} \tag{146}$$

Rearrange the index notation, and we can get the final boundary integral equation of three-dimensional stokes flow:

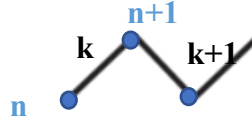
$$\begin{aligned}
u_j(\mathbf{x}^0) = & -\frac{1}{8\pi\mu} \iint S_{ji}(\mathbf{x}^0, \mathbf{x}) f_i(\mathbf{x}) dS(\mathbf{x}) \\
& + \frac{1}{8\pi} \iint u_i(\mathbf{x}) T_{ijk}(\mathbf{x}, \mathbf{x}^0) n_k(\mathbf{x}) dS(\mathbf{x})
\end{aligned} \tag{147}$$

The velocity can be expressed in terms of a combination of single and double-layer potential. However, it is common to ignore the effect of double-layer potential when the structures are stiff, and the single-layer potential dominates in the boundary integral, and stresslet decays very rapidly over distance. We will only consider the single-layer potential, Stokeslet, in the boundary integral equation.

$$u_j(\mathbf{x}^0) \cong -\frac{1}{8\pi\mu} \iint_s S_{ji}(\mathbf{x}^0, \mathbf{x}) f_i(\mathbf{x}) dS(\mathbf{x}) \tag{148}$$

E. Geometric interpolations [10]

In our equation of motion, we only have discrete nodal values. But the boundary element method requires integration over the domains between nodal values. We, therefore, require interpolation to provide a continuous domain for evaluating the integral. In the following, we use index k to represent variables associated with the k th elements, and index n represents values associated with the nodes. The whole domain can be interpolated through the following parametrized piecewise polynomials [10]:



$$\mathbf{r}_k(s) = [x_k(s), y_k(s), z_k(s)]$$

$$\begin{aligned} x_k(s) &= a_k(s - s_n)^3 + b_k(s - s_n)^2 + c_k(s - s_n) + x_n^G \\ y_k(s) &= a'_k(s - s_n)^3 + b'_k(s - s_n)^2 + c'_k(s - s_n) + y_n^G \\ z_k(s) &= a''_k(s - s_n)^3 + b''_k(s - s_n)^2 + c''_k(s - s_n) + z_n^G \end{aligned} \quad (149)$$

Where 's' is the arch length of the line integrals. s_k denotes a continuous variable associated with the k th element. s_n denotes a discrete nodal value. We use $x_k(s)$ as an example for illustrative purposes, and the same applies to $y_k(s)$, $z_k(s)$. We have three unknown coefficients, a_k , b_k , c_k , for each of the piecewise polynomials $x_k(s)$. We use the following three conditions to form constraints on solving the unknown coefficients to ensure the domain is smoothly-connected.

1. Continuous function:

$$x_k(s_{n+1}) = x_{n+1}^G$$

2. Continuous slope:

$$\left. \frac{dx_k(s)}{ds} \right|_{s_{n+1}} = \left. \frac{dx_{k+1}(s)}{ds} \right|_{s_{n+1}}$$

3. Continuous curvature:

$$\left. \frac{d^2 x_k(s)}{ds^2} \right|_{s_{n+1}} = \left. \frac{d^2 x_{k+1}(s)}{ds^2} \right|_{s_{n+1}}$$

The relation for b_k after satisfying the above constraints for $k = 1, \dots, N - 1$ can be established as:

$$\frac{h_k}{3} b_k + 2 \frac{h_k + h_{k+1}}{3} b_{k+1} + \frac{h_{k+1}}{3} b_{k+2} = \frac{x_{k+2}^G - x_{k+1}^G}{h_{k+1}} - \frac{x_{k+1}^G - x_k^G}{h_k}, \quad h_k = s_{k+1} - s_k \quad (150)$$

The stencil in equation (150) is a tridiagonal matrix and can be easily solved using linear algebra routine with boundary conditions:

$$\text{clamped end: } b_1 = -\frac{1}{2} b_2 + \frac{3}{2h_1} \left(\frac{x_2^G - x_1^G}{h_1} \right) \quad (151)$$

$$\text{free end: } b_{N+1} = 0 \quad (152)$$

After we solve for the values of b_i , the values of a_i and c_i can found through substitution:

$$a_k = \frac{b_{k+1} - b_k}{3h_k} \quad (153)$$

$$c_k = \frac{x_{k+1}^G - x_k^G}{h_k} - \frac{1}{3} h_k (b_{k+1} + 2b_k) \quad (154)$$

Once we obtain these coefficients, we can obtain the centerline position of the curves, and also the differentials of the line integrals which can be rewritten in the following parametrized form:

$$dl(\mathbf{r}_k) = \sqrt{dx^2 + dy^2 + dz^2} = h_k(s) ds_k \quad (155)$$

$$h_k(s) = \left([3a_k(s - s_n)^2 + 2b_k(s - s_n) + c_k]^2 + [3a'_k(s - s_n)^2 + 2b'_k(s - s_n) + c'_k]^2 + [3a''_k(s - s_n)^2 + 2b''_k(s - s_n) + c''_k]^2 \right)^{\frac{1}{2}} \quad (156)$$

Now we have a set of relations to map the discrete nodal values into continuous smoothly connected domains that are ready for computing the integrals.

F. Mathematical lemmas

We provide a reference table of several important mathematical lemmas that has been used frequently in fundamental solutions derivations in appendix B for chapter 3.

$$\delta_{ii} = 3, \quad \delta_{ij} = \frac{\partial x_i}{\partial x_j} \quad (157)$$

$$\frac{\partial \hat{x}_j}{\partial x_i} = \frac{\partial}{\partial x_i} (x_j - x_j^0) = \delta_{ij} \quad (158)$$

$$\frac{\partial f(r)}{\partial x_i} = \frac{df}{dr} \frac{\partial r}{\partial x_i} \quad (159)$$

$$\frac{\partial r}{\partial x_i} = \frac{1}{2\sqrt{\hat{x}_j \hat{x}_j}} \frac{\partial \hat{x}_j \hat{x}_j}{\partial x_i} = \frac{1}{2r} \left(\hat{x}_j \frac{\partial \hat{x}_j}{\partial x_i} + \hat{x}_j \frac{\partial \hat{x}_j}{\partial x_i} \right) = \frac{1}{r} \hat{x}_j \frac{\partial \hat{x}_j}{\partial x_i} = \frac{\hat{x}_j \delta_{ij}}{r} = \frac{\hat{x}_i}{r} \quad (160)$$

$$\frac{\partial^2 r}{\partial x_i \partial x_j} = \frac{\partial}{\partial x_i} \frac{\hat{x}_j}{r} = -\frac{\hat{x}_j \hat{x}_i}{r^3} + \frac{1}{r} \delta_{ij} \quad (161)$$

$$\frac{\partial^2 r}{\partial x_i^2} = \frac{\partial}{\partial x_i} \frac{\hat{x}_i}{r} = -\frac{\hat{x}_i \hat{x}_i}{r^3} + \frac{1}{r} \delta_{ii} = -\frac{r^2}{r^3} + \frac{3}{r} = \frac{2}{r} \quad (162)$$

$$\frac{\partial}{\partial x_i} \frac{1}{r} = -\frac{\hat{x}_i}{r^3} \quad (163)$$

$$\frac{\partial}{\partial x_i} \frac{\partial}{\partial x_j} \frac{1}{r} = 3 \left(\frac{\hat{x}_i \hat{x}_j}{r^5} - \frac{\delta_{ij}}{3r^3} \right) \quad (164)$$

Stresslet derivation:

$$T_{ijk} = -\delta_{ik} \frac{2x_j}{r^3} + \frac{\partial S_{ij}}{\partial x_k} + \frac{\partial S_{kj}}{\partial x_i} \quad (165)$$

$$\frac{\partial S_{ij}}{\partial x_k} = -\frac{x_k}{r^3} \delta_{ij} + \frac{1}{r^3} (x_i \delta_{jk} + x_j \delta_{ik}) - 3 \frac{x_j x_i x_k}{r^5} \quad (166)$$

$$\frac{\partial S_{kj}}{\partial x_i} = -\frac{x_i}{r^3} \delta_{kj} + \frac{1}{r^3} (x_k \delta_{ji} + x_j \delta_{ki}) - 3 \frac{x_j x_k x_i}{r^5} \quad (167)$$

$$T_{ijk} = -\delta_{ik} \frac{2x_j}{r^3} - \frac{x_k}{r^3} \delta_{ij} + \frac{1}{r^3} (x_i \delta_{jk} + x_j \delta_{ik}) - 3 \frac{x_j x_i x_k}{r^5} - \frac{x_i}{r^3} \delta_{kj} + \frac{1}{r^3} (x_k \delta_{ji} + x_j \delta_{ki}) - 3 \frac{x_j x_k x_i}{r^5} \quad (168)$$

$$T_{ijk} = \frac{2x_i}{r^3} \delta_{jk} - 3 \frac{x_j x_i x_k}{r^5} - \frac{2x_i}{r^3} \delta_{kj} - 3 \frac{x_j x_k x_i}{r^5} \quad (169)$$

$$T_{ijk} = -6 \frac{x_j x_k x_i}{r^5} \quad (170)$$

References

- [1] J. Dobson, A. Kumar, L. F. Willis, R. Tuma, D. R. Higazi, R. Turner, D. C. Lowe, A. E. Ashcroft, S. E. Radford, N. Kapur, and D. J. Brockwell, *Proc. Natl. Acad. Sci. U. S. A.* **114**, 4673 (2017).
- [2] H. Lin, R. Bhatia, and R. Lal, *FASEB J.* **15**, 2433 (2001).
- [3] I. A. Houghton, J. R. Koseff, S. G. Monismith, and J. O. Dabiri, *Nature* **556**, 497 (2018).
- [4] B. Piorek, Á. Mechler, R. Lal, P. Freudenthal, C. Meinhart, and S. Banerjee, *Appl. Phys. Lett.* **89**, (2006).
- [5] A. Mechler, B. Piorek, R. Lal, and S. Banerjee, *Appl. Phys. Lett.* **85**, 3881 (2004).
- [6] A. Quist, A. Chand, S. Ramachandran, D. Cohen, and R. Lal, *Lab Chip* **6**, 1450 (2006).
- [7] C. S. Peskin, *Acta Numer.* **11**, 479 (2002).
- [8] D. J. Smith, *Proc. R. Soc. A Math. Phys. Eng. Sci.* **465**, 3605 (2009).
- [9] B. Audoly, in *RSC Soft Matter* (Royal Society of Chemistry, 2016), pp. 1–24.
- [10] C. Pozrikidis, *A Practical Guide to Boundary Element Methods with the Software Library BEMLIB* (Chapman & Hall/CRC, 2002).
- [11] M. K. Jawed, A. Novelia, and O. M. O’Reilly, *A Primer on the Kinematics of Discrete Elastic Rods* (Springer International Publishing, Cham, 2018).
- [12] K. Jawed,
https://www.cs.cmu.edu/afs/cs.cmu.edu/academic/class/16311/www/s17/syllabus/ppp/Rods_Mechanics_MK.pdf
- [13] D. Barthès-biesel, *Microhydrodynamics and Complex Fluids*. (CRC Pr I Llc, 2017).
- [14] M. D. Graham, *Microhydrodynamics, Brownian Motion, and Complex Fluids* (Cambridge University Press, 2018).
- [15] C. Pozrikidis, *Boundary Integral and Singularity Methods for Linearized Viscous Flow* (Cambridge Texts in Applied Mathematics, 1992).
- [16] É. Guazzelli and J. F. Morris, *A Physical Introduction to Suspension Dynamics* (Cambridge Texts in Applied Mathematics, 2011).
- [17] J. R. Blake, *Math. Proc. Cambridge Philos. Soc.* **70**, 303 (1971).

- [18] R. Cortez, L. Fauci, and A. Medovikov, *Phys. Fluids* **17**, (2005).
- [19] J. Ainley, S. Durkin, R. Embid, P. Boindala, and R. Cortez, *J. Comput. Phys.* **227**, 4600 (2008).
- [20] C. Pozrikidis, *Numerical Computation in Science and Engineering* (Oxford University Press, 2008).